

Regularized and Smooth Double Core Tensor Factorization for Heterogeneous Data*

Davoud Ataee Tarzanagh[†] and George Michailidis[‡]

Abstract. We introduce a general tensor model suitable for data analytic tasks for *heterogeneous* data sets, wherein there are joint low-rank structures within groups of observations, but also discriminative structures across different groups. To capture such complex structures, a double core tensor (DCOT) factorization model is introduced together with a family of smoothing loss functions. By leveraging the proposed smoothing function, the model accurately estimates the model factors, even in the presence of missing entries. A linearized ADMM method is employed to solve regularized versions of DCOT factorizations, that avoid large tensor operations and large memory storage requirements. Further, we establish theoretically its global convergence, together with consistency of the estimates of the model parameters. The effectiveness of the DCOT model is illustrated on several real-world examples including image completion, recommender systems, subspace clustering and detecting modules in heterogeneous Omics multi-modal data, since it provides more insightful decompositions than conventional tensor methods.

Key words. Double core tensor factorization, heterogeneity, smoothing loss functions, ADMM, regularization

1. Introduction. Tensor factorizations have received increased attention over the last decade, due to new technical developments, as well as novel applications - see [40, 21, 69, 72] and references therein. Popular decompositions include Tucker [78, 79], Canonical Polyadic (CP) [17], higher-order SVD (HOSVD) [22, 23], tensor train (TT) [60] and tensor SVD (t-SVD) [38]. Nevertheless, there is limited knowledge about the properties of the Tucker and CP ranks; further, computing such ranks has been shown to be a NP-complete problem [29]. The ill-posedness of the best low-rank approximation of a tensor was investigated in [24], while upper and lower bounds for tensor ranks have been studied in [3]. In fact, determining or even bounding the rank of an arbitrary tensor is quite difficult in contrast to the matrix rank [4].

In many data analysis applications where tensor decompositions are extensively used, the multi-dimensional data exhibit (i) heterogeneity, (ii) missing values and (iii) admit sparse representations. The literature to date has addressed the 2nd and 3rd issues, as briefly discussed next. Missing values are ubiquitous in link prediction, recommender systems, chemometrics, image and video analytics applications. To that end, tensor completion methods were developed to address this issue [50, 41, 95, 18, 75]. The standard assumption underpinning such methods is that entries are missing at random and that the data admit a low-rank decomposition. However, on many occasions additional *similarity* information is available, which may aid in improving the accuracy of tensor completion methods, especially in the presence of large number of missing entries. For example, Narita et al. [56] proposed two regularization methods

*Submitted.

Funding: This work was supported in part by NSF grants . . . and by the UF Informatics Institute.

[†]Department of Mathematics & UF Informatics Institute, University of Florida, Gainesville, FL, tarzanagh@ufl.edu.

[‡]Department of Statistics & UF Informatics Institute, University of Florida, Gainesville, FL, gmichail@ufl.edu.

called “within-mode regularization” and “cross-mode regularization”, to incorporate auxiliary similarity information in tensor factorization. The key idea is to construct within-mode or cross-mode similarity matrices and incorporate them as smooth regularizers and then combining them with a Tucker decomposition to solve the tensor completion problem. A similar idea was also explored in [5, 18, 28].

Multi-way data often admit sparse representations. Due to the equivalence of the constrained Tucker model and the Kronecker representation of a tensor, the latter can be represented by separable sparse Kronecker dictionaries or g. A number of dictionary learning methods have been proposed in the literature - see, e.g. [30, 62, 67, 6] and associated algorithms. Further, recent work ([67]) shows that the sample complexity of dictionary learning for tensor data can be significantly lower than that for unstructured data, also supported by empirical evidence [62].

However, in a number of applications *heterogeneity* is also present in the data. For example, in context-aware recommender systems that predict users’ preferences, the user base exhibits heterogeneity due to different background and other characteristics. Note that such information can be a priori extracted from the available data. Similarly, image data exhibit heterogeneity due to differences in lighting and posing, which again can be extracted a priori from available metadata and utilized at analysis time. Analogous issues also are present in time varying data, wherein strong correlations can be seen across subsets of time points. A number of motivating examples are discussed in detail in Subsection 2.3, and how this paper addresses heterogeneity by adding an additional core in the tensor decomposition. Note that a standard low-rank factorization of the tensor data would not suffice, since the extracted factors would not accurately reflect the joint structure across modes. Hence, to address heterogeneity in tensor factorizations, we introduce a novel decomposition of the core tensor into a global homogeneous and local (subject specific) heterogeneous cores. The latter encode a priori available information on the *presence* and *structure* of heterogeneity on the data sets under consideration.

Hence, the *key contributions* of this work are:

- I. The development of a novel *supervised* tensor decomposition, coined *Double Core Tensor Decomposition* (DCOT), wherein the core tensor comprises of the superposition of a *homogeneous* and *heterogeneous* (subject specific) cores. This decomposition captures local structure present due to variations in similarities across subjects/objects in the data.
- II. The DCOT model is enhanced with a new tensor smoothing loss function. Specifically, a similarity function is introduced to capture neighborhood information from the data tensor to improve the accuracy of the decompositions, as well as the convergence rate of the algorithm employed for obtaining the decomposition. We show both theoretical and computational advantages of the proposed smoothing technique in comparison to Kronecker Laplacian-based methods [56, 5, 18, 28] and the generalized CP (GCP) model [34].
- III. A new linearized ADMM method for the DCOT model is developed that can handle both non-convex constraints and loss functions and its global convergence under the posited tensor smoothing loss function is established. To the best of our knowledge, despite the

wide use and effectiveness of ADMM for tensor factorization tasks [50, 96, 19, 84, 6] its global convergence does not seem to be available for tensor problems.

Finally, we illustrate the implementation of DCOT and the speed and robustness of the proposed linearized ADMM algorithm on a number of synthetic data sets, as well as analytic tasks involving large scale heterogeneous tensor data.

The remainder of the paper is organized as follows: the DCOT formulation is presented in Section 2 together with illustrative motivating examples. The linearized ADMM algorithm and its convergence properties are presented in Section 3, while the numerical performance of the DCOT model and the algorithm together with applications are discussed in Section 5. Proofs and other technical results are delegated to the Appendix.

Notation. Relevant mathematical concepts, including basic algebra and operations related to tensors are provided in the Appendix (see Table 5.5).

2. A Double Core Tensor Factorization (DCOT). We start by introducing the DCOT model.

Definition 2.1 (DCOT). Given an N -way tensor $\mathbf{Z} \in \mathbb{R}^{I_1 \times I_2 \times \dots \times I_N}$ with M subjects/units each containing m_π subgroups for $m = 1, \dots, M$, its DCOT decomposition is given by

$$\begin{aligned} \mathbf{Z} &= \sum_{r_1=1}^{R_1} \dots \sum_{r_N=1}^{R_N} (g_{r_1 \dots r_N} + h_{r_1 \dots r_N}) \mathbf{u}_{r_1}^{(1)} \circ \dots \circ \mathbf{u}_{r_N}^{(N)} \\ &= (\mathcal{G} + \mathcal{H}) \times_1 \mathbf{U}^{(1)} \times_2 \mathbf{U}^{(2)} \dots \times_N \mathbf{U}^{(N)}, \end{aligned}$$

where $\mathbf{U}^{(n)} = [\mathbf{u}_1^{(n)}, \mathbf{u}_2^{(n)}, \dots, \mathbf{u}_{R_n}^{(n)}] \in \mathbb{R}^{I_n \times R_n}$, is the n -th factor matrix for $n = 1, 2, \dots, N$, consisting of latent components $\mathbf{u}_1^{(n)}$; $\mathcal{G} \in \mathbb{R}^{R_1 \times R_2 \times \dots \times R_N}$ is a global core tensor reflecting the connections (or links) between the latent components and factor matrices; and \mathcal{H} is another core tensor reflecting the joint connections between the latent components in each subject. Specifically, for each subject $m \in [M]$, we have

$$\mathcal{H}_{m_1} = \mathcal{H}_{m_2} = \dots = \mathcal{H}_{m_\pi}.$$

In Definition 2.1, the N -tuple (R_1, R_2, \dots, R_N) with $R_n = \text{rank}(\mathbf{Z}_{(n)})$ is called the multi-linear rank of \mathbf{Z} . For a core tensor of minimal size, R_1 is the column rank (the dimension of the subspace spanned by mode-1 fibers), R_2 is the row rank (the dimension of the subspace spanned by mode-2 fibers), and so on. An important difference from the matrix case is that the values of R_1, R_2, \dots, R_N can be different for $N \geq 3$. Note that similar to the Tucker decomposition [78, 79], DCOT factorization is said to be independent, if each of the factor matrices has full column rank; a DCOT decomposition is said to be orthonormal if each of the factor matrices has orthonormal columns. It is worth mentioning that decomposition (2.1) can be expressed in a matrix form as:

$$(2.1) \quad \mathbf{Z}_{(n)} = \mathbf{U}^{(n)} (\mathbf{G}_{(n)} + \mathbf{H}_{(n)}) \left(\bigotimes_{k \neq n} \mathbf{U}^{(k)} \right)^\top.$$

The DCOT model formulation provides a generic tensor decomposition that encompasses many other popular tensor decomposition models. Indeed, when $\mathcal{H} = 0$ and $\mathbf{U}^{(n)}$, for

$n = 1, 2, \dots, N$ are orthogonal, (2.1) corresponds to the orthonormal Tucker decomposition, which is also known as the higher-order SVD (HOSVD) [22, 23]. The CP decomposition of a tensor is another important variant that leads to the definition of CP rank [17]. The latter can also be considered as a special case of the DCOT model with super-diagonal core tensors. Further, the CP rank of a tensor equals that of its DCOT core.

Next, we propose an estimation method associated with the DCOT model. Let \mathbf{X} be a data tensor that admits a DCOT decomposition and $F(s^h, \mathbf{X}; \mathbf{Z})$ be a smoothing statistical loss function (introduced in subsection 2.1) that depends on an unknown parameter \mathbf{Z} and regulated by a smoothing parameter s^h (details discussed in subsection 2.1). To estimate \mathbf{Z} from data, we propose the “DCOT” estimator given by

$$(2.2) \quad \hat{\mathbf{Z}} := (\hat{\mathbf{G}} + \hat{\mathbf{H}}) \times_1 \hat{\mathbf{U}}^{(1)} \times_2 \hat{\mathbf{U}}^{(2)} \dots \times_N \hat{\mathbf{U}}^{(N)},$$

where $\hat{\mathbf{Z}}$ is determined by solving the following penalized optimization problem:

$$(2.3) \quad \begin{aligned} \min_{\mathcal{T}} \quad & F(s^h, \mathbf{X}; \mathbf{Z}) + \lambda_1 J_1(\mathbf{G}) + \lambda_2 J_2(\mathbf{H}) + \sum_{n=1}^N \lambda_{3,n} J_{3,n}(\mathbf{U}^{(n)}), \\ \text{s.t.} \quad & \mathbf{Z} = (\mathbf{G} + \mathbf{H}) \times_1 \mathbf{U}^{(1)} \times_2 \mathbf{U}^{(2)} \dots \times_N \mathbf{U}^{(N)}, \quad \mathcal{T} \in \Gamma(\mathcal{T}). \end{aligned}$$

In the formulation of the problem, $\mathcal{T} = (\mathbf{Z}, \mathbf{G}, \mathbf{H}, \mathbf{U}^{(1)}, \mathbf{U}^{(2)}, \dots, \mathbf{U}^{(N)})$ denotes the collection of optimization variables, $\{J_1(\cdot), J_2(\cdot), J_{3,1}(\cdot), J_{3,2}(\cdot), \dots, J_{3,N}(\cdot)\}$ are penalty functions; $\{\lambda_1, \lambda_2, \lambda_{3,1}, \lambda_{3,2}, \dots, \lambda_{3,N}\}$ are penalty tuning parameters; and $\Gamma(\mathcal{T})$ is the parameter space for \mathcal{T} . Throughout, we impose the following set of assumptions for problem (2.3).

- Assumption 2.2.** (i) $J_1 : \mathbb{R}^{R_1 \times R_2 \times \dots \times R_N} \rightarrow (-\infty, \infty]$, $J_2 : \mathbb{R}^{R_1 \times R_2 \times \dots \times R_N} \rightarrow (-\infty, \infty]$ and $J_{3,n} : \mathbb{R}^{N_n \times R_n} \rightarrow (-\infty, \infty]$ are proper and lower semi-continuous such that $\inf_{\mathbb{R}^{R_1 \times R_2 \times \dots \times R_N}} J_1 > -\infty$, $\inf_{\mathbb{R}^{R_1 \times R_2 \times \dots \times R_N}} J_2 > -\infty$ and $\inf_{\mathbb{R}^{I_n \times R_n}} J_{3,n} > -\infty$ for $n = 1, 2, \dots, N$.
(ii) $F(s^h, \mathbf{X}; \mathbf{Z}) : \mathbb{R}^{I_1 \times I_2 \times \dots \times R^{IN}} \rightarrow \mathbb{R}$ is differentiable and $\inf_{\mathbb{R}^{I_1 \times I_2 \times \dots \times R^{IN}}} F > -\infty$.
(iii) $\nabla F(s^h, \mathbf{X}; \mathbf{Z})$ is Lipschitz continuous with moduli L , that is,

$$\|\nabla F(s^h, \mathbf{X}; \mathbf{Z}^1) - \nabla F(s^h, \mathbf{X}; \mathbf{Z}^2)\|_F^2 \leq L \|\mathbf{Z}^1 - \mathbf{Z}^2\|_F^2, \quad \text{for all } \mathbf{Z}^1, \mathbf{Z}^2.$$

Assumption (i) is very general and satisfied by many constraints (e.g. indicator functions) and penalty functions including ℓ_1 and nuclear norms. Assumptions (ii)-(iii) are leveraged to obtain the proposed DCOT factorization and a globally convergent linearized ADMM for general non-convex losses.

Remark 2.3. Note that separate identification of \mathbf{G} and \mathbf{H} is not required; the DCOT estimator is designed to automatically recover the combination $\hat{\mathbf{G}} + \hat{\mathbf{H}}$ that leads to optimal prediction of $\mathbf{G} + \mathbf{H}$. Nevertheless, it can be beneficial from both a convergence and interpretation viewpoint. To that end, we show in Section 3 that Assumption 2.2 provides sufficient conditions to achieve identifiable cores based on a linearized multi-block ADMM approach.

2.1. Smooth loss functions for DCOT factorization. In this section, we introduce a new class of smoothing loss functions for DCOT factorization that in addition to the unit/subject information reflected in the \mathbf{H} core, it incorporates more nuanced information in the form

of similarities between tensor fibers for each unit/subject under consideration. To that end, following common approaches in non-parametric statistics [83, 77, 26, 45, 8], we define next the smoothing loss function used in this work. Our proposed smoothing approach is different from these studies, since we rely on network-based joint similarity information and multi-dimensional data analysis.

2.2. A smoothing function based on tensor similarity and tensor labels. The proposed loss function incorporates both *tensor similarity* information, as well as subgroup or label information. For example, in dictionary learning problems, in addition to using similarity information between data points, we also associate label information (0-1 tensor label) with each dictionary item (fibers of the dictionary tensor) to enforce discriminability in sparse codes during the dictionary learning process [37]. In recommender systems, the proposed loss function is constructed based on the closeness between continuous covariates in addition to a user-item specific label tensor [27]. In many imaging applications, additional variables of interest are available for multiway data objects. For instance, [42] provide several attributes for the images in the Faces in the Wild database, which describe the individual (e.g., gender and race) or their expression (e.g., smiling / not smiling). It is shown in [52] that incorporating such additional variables can improve both the accuracy and the interpretation of the results.

Given an N -way data tensor \mathcal{X} , assume we have additional information on each item/subject in the data, encoded by an N -way tensor \mathcal{Y} . Assume pairwise similarities $s_{i_1 \dots i_N, j_1 \dots j_N}$ between the fibers of \mathcal{Y} are available. Each $s_{i_1 \dots i_N, j_1 \dots j_N}$ indicates how well fibers of \mathcal{Y} represent fibers of \mathcal{X} ; i.e., the smaller the value of $s_{i_1 \dots i_N, j_1 \dots j_N}$ is, the better \mathcal{Y} represents \mathcal{X} . For example, we can define tensor similarities as joint-fiber similarities by

$$(2.4) \quad s_{i_1 \dots i_N, j_1 \dots j_N}^h = s_{i_1, j_1}^h c_{i_1, j_1} \cdots s_{i_N, j_N}^h c_{i_N, j_N},$$

where $h > 0$ is the window size and each $\{s_{i_n, j_n}\}$ measures the distance between the fibers (i_n, j_n) for $n = 1, \dots, N$; c_{i_n, j_n} is a label consistent constraint which is set to a value close to 1 if fibers i_n and j_n share the same labels or belong to the same subgroups, and close to 0, otherwise. We also note that a large value of h implies that $s_{i_1 \dots i_N, j_1 \dots j_N}^h$ has a wide range, while a small h corresponds to a narrow range for $s_{i_1 \dots i_N, j_1 \dots j_N}^h$.

When appropriate vector-space representations of fibers of \mathcal{Y} are given, we can compute similarities using a predefined function. Such functions the encoding error $-s_{i_n, j_n}^h = K(h^{-1} \|\mathbf{A}\mathbf{y}_{i_n} - \mathbf{y}_{j_n}\|_2)$ for an appropriate \mathbf{A} -, the Euclidean distance $-s_{i_n, j_n}^h = K(h^{-1} \|\mathbf{y}_{i_n} - \mathbf{y}_{j_n}\|_2)$ -, or a truncated quadratic $-s_{i_n, j_n}^h = \min\{\xi, K(h^{-1} \|\mathbf{y}_{i_n} - \mathbf{y}_{j_n}\|_2)\}$ -, where ξ is some constant and K denotes a kernel matrix [77]. However, we may be given or can compute similarities without having access to vector-space representations; such instances include edges in a social network graph, subjective pairwise comparisons between images, or similarities between sentences computed via a string kernel [25].

Remark 2.4. *It is important to note that we can work with the sum of similarities instead of their product in (2.4), simply by setting*

$$s_{i_1 \dots i_N, j_1 \dots j_N}^h = s_{i_1, j_1}^h c_{i_1, j_1} + \cdots + s_{i_N, j_N}^h c_{i_N, j_N}$$

in our formulation to form joint similarities.

Remark 2.5. In contrast to [56, 5, 18, 28], we do not restrict \mathcal{X} and \mathcal{Y} to consist of same type of elements or be identical. For example, \mathcal{Y} can be a set of covariates for each subject/sample and \mathcal{X} be a set of subjects/samples. This generalization also allows to reduce the cost of computing and storing similarities. Specifically, when dealing with a large dataset, we can select a small random subset of the dataset as \mathcal{Y} with the target set \mathcal{X} being the entire dataset.

2.2.1. Generalized smoothing tensor loss functions. Next, we define a smoothing loss functions by looking at the statistical likelihood of a model for a given data tensor. Assume that we have a parameterized probability density function or probability mass function that gives the likelihood of each entry, i.e.,

$$x_{i_1 \dots i_N} \sim p(x_{i_1 \dots i_N} | \theta_{i_1 \dots i_N}) \text{ where } \ell(\theta_{i_1 \dots i_N}) = z_{i_1 \dots i_N}.$$

Here, $x_{i_1 \dots i_N}$ is a realization of a random variable and $\ell(\cdot)$ is an invertible *link function* that connects the model parameter $z_{i_1 \dots i_N}$ and the corresponding *natural parameter* of the distribution, $\theta_{i_1 \dots i_N}$. Our goal is to obtain the maximum likelihood estimate \mathbf{Z} . Assuming that the samples are independent and identically distributed, we can obtain \mathbf{Z} by solving

$$(2.5) \quad \max_{\mathbf{Z}} L(\mathbf{X}; \mathbf{Z}) \equiv \prod_{i_1, \dots, i_N \in \Omega} p(x_{i_1 \dots i_N} | \theta_{i_1 \dots i_N}) \text{ where } \ell(\theta_{i_1 \dots i_N}) = z_{i_1 \dots i_N}.$$

where Ω is an index set of observed tensor components.

Working with the log-likelihood, and using the proposed similarity function s^h , we obtain the following minimization problem

$$(2.6) \quad \min_{\mathbf{Z}} \left\{ F(s^h, \mathbf{X}; \mathbf{Z}) = \frac{1}{\Omega} \sum_{i_1, \dots, i_N \in \Omega} f(s_{i_1 \dots i_N}^h, z_{i_1 \dots i_N}, x_{i_1 \dots i_N}) \right\},$$

where

$$(2.7) \quad f(s_{i_1 \dots i_N}^h, z_{i_1 \dots i_N}, x_{i_1 \dots i_N}) = - \sum_{j_1, \dots, j_N \in \Omega} s_{i_1 \dots i_N, j_1 \dots j_N}^h \log(p(x_{i_1 \dots i_N} | \ell^{-1}(z_{i_1 \dots i_N}))),$$

is a smoothing probability density function.

Next, we present various loss functions, corresponding to different types of data; e.g., numerical, binary, count.

2.2.2. Numerical data. For such data, under the assumption of low-rank structure, we can represent them as

$$(2.8) \quad x_{i_1 \dots i_N} = z_{i_1 \dots i_N} + \epsilon_{i_1 \dots i_N} \text{ with } \epsilon_{i_1 \dots i_N} \sim \mathcal{N}(\mu, \sigma^2) \text{ for all } i_1 \dots i_N \in \Omega.$$

where $\mathcal{N}(\mu, \sigma^2)$ denotes the normal or Gaussian distribution with mean μ and variance σ^2 ¹.

It follows from (2.8) that:

$$x_{i_1 \dots i_N} \sim \mathcal{N}(\mu_{i_1 \dots i_N}, \sigma^2) \text{ with } \mu_{i_1 \dots i_N} = z_{i_1 \dots i_N}.$$

Under assumption (2.8), the proposed smoothing loss function is given by

$$(2.9) \quad f(s_{i_1 \dots i_N}^h, z_{i_1 \dots i_N}, x_{i_1 \dots i_N}) = \sum_{j_1, \dots, j_N \in \Omega} s_{i_1 \dots i_N, j_1 \dots j_N}^h (z_{i_1 \dots i_N} - x_{i_1 \dots i_N})^2.$$

¹We assume σ is constant across all entries.

2.2.3. Binary data. The standard assumption of a data generating mechanism for such data is the Bernoulli distribution; specifically, a binary random variable $x \in \{0, 1\}$ is Bernoulli distributed with parameter $\rho \in [0, 1]$ if ρ is the probability of obtaining a value of 1 and $(1 - \rho)$ is the probability of obtaining a value of zero. The probability mass function is given by

$$(2.10) \quad p(x|\rho) = \rho^x(1 - \rho)^{(1-x)}, \quad x \in \{0, 1\}, \quad x \sim \text{Bernoulli}(\rho).$$

A reasonable model for a binary data tensor \mathfrak{X} is

$$(2.11) \quad x_{i_1 \dots i_N} \sim \text{Bernoulli}(\rho_{i_1 \dots i_N}), \quad \text{where } \ell(\rho_{i_1 \dots i_N}) = z_{i_1 \dots i_N}.$$

A common option for the link function $\ell(\rho)$ is to work with the log-odds [34], i.e.,

$$(2.12) \quad \ell(\rho) = \log\left(\frac{\rho}{1 - \rho}\right).$$

Substituting (2.12) into (2.6), we get the following smoothing function

$$f(s_{i_1 \dots i_N}^h, z_{i_1 \dots i_N}, x_{i_1 \dots i_N}) = \sum_{j_1, \dots, j_N \in \Omega} s_{i_1 \dots i_N, j_1 \dots j_N}^h (\log(1 + e^{z_{i_1 \dots i_N}}) - x_{i_1 \dots i_N} z_{i_1 \dots i_N}),$$

where $x_{i_1 \dots i_N} \in \{0, 1\}$ and the associated probability is $\rho = e^{z_{i_1 \dots i_N}} / (1 + e^{z_{i_1 \dots i_N}})$.

2.2.4. Count data. For such data, it is common to model them as Poisson distributed. The probability mass function for a Poisson distribution with mean λ is given by

$$(2.13) \quad p(x|\lambda) = \frac{e^{-\lambda} \lambda^x}{x!} \quad \text{for } x \in \mathbb{N}.$$

If we use the identity link function ($\ell(\lambda) = \lambda$) and (2.13) in (2.6), then we obtain

$$(2.14) \quad f(s_{i_1 \dots i_N}^h, z_{i_1 \dots i_N}, x_{i_1 \dots i_N}) = \sum_{j_1, \dots, j_N \in \Omega} s_{i_1 \dots i_N, j_1 \dots j_N}^h (z_{i_1 \dots i_N} - x_{i_1 \dots i_N} \log z_{i_1 \dots i_N}),$$

where $x_{i_1 \dots i_N} \in \mathbb{N}$ and $z_{i_1 \dots i_N} \geq 0$.

2.2.5. Positive continuous data. There are several distributions for handling nonnegative continuous data: Gamma, Rayleigh, and even Gaussian with nonnegativity constraints. Next, we consider the Gamma distribution which is appropriate for strictly positive data. For $x > 0$, the probability density function is given by

$$(2.15) \quad p(x|t, \theta) = \frac{x^{t-1} e^{-x/\theta}}{\Gamma(t) \theta^t},$$

where the parameters t and θ are positive real quantities as is the variable x and $\Gamma(\cdot)$ is the Gamma function.

A common choice for the link function is $\ell(t, \theta) = \theta/t$ which induces a positivity constraint on $z_{i_1 \dots i_N}$. Assume t is constant across all entries. Plugging the link function and (2.15) into (2.6) and removing the constant terms yields the smoothing loss function

$$(2.16) \quad f(s_{i_1 \dots i_N}^h, z_{i_1 \dots i_N}, x_{i_1 \dots i_N}) = \sum_{j_1, \dots, j_N \in \Omega} s_{i_1 \dots i_N, j_1 \dots j_N}^h (\log(z_{i_1 \dots i_N}) + x_{i_1 \dots i_N} / z_{i_1 \dots i_N}),$$

where $x_{i_1 \dots i_N}$ and $z_{i_1 \dots i_N}$ are both positive. In practice we use $z_{i_1 \dots i_N} \geq 0$ and replace $z_{i_1 \dots i_N}$ with $z_{i_1 \dots i_N} + \epsilon$ (with small ϵ) in the loss function (2.16).

2.3. Motivating examples and applications of the DCOT Model. Next, we discuss a number of motivating examples for DCOT and the associated smoothing loss function.

2.3.1. Context-aware recommender systems. Recommender systems predict users' preferences across a set of items based on large past usage data, while also leveraging information from similar users. In multilayer recommender systems, a tensor based analysis is beneficial due to its flexibility to accommodate contextual information from data, and is also regarded as effective in developing context-aware recommender systems (CARS) [1, 2, 27, 9]. Besides user and item information available in traditional recommender systems [43, 81, 10], multilinear recommender systems also use additional contextual variables, including geolocation data, time stamps, store information, etc. Although CARS are capable of utilizing such additional information and thus furnishing more accurate recommendations, they are also hampered by the so-called "cold-start" problem, wherein not sufficient information is available on new users, items or contexts. To that end, the following penalized variant of (2.3)

$$(2.17) \quad F(s^h, \mathbf{X}; \mathbf{Z}) + \lambda_1 \|\mathbf{G}\|_F^2 + \lambda_2 \|\mathbf{H}\|_F^2 + \lambda_3 \|\mathbf{U}\|_F^2,$$

is helpful, where λ_i for $i = 1, 2, 3$ denote tuning parameters.

The loss function (2.17) enables pooling information from neighboring (i_1, i_2, \dots, i_N) points, through similarity functions s^h . Further, it addresses satisfactorily the "cold start" problem, by leveraging information from similar users in similar contextual settings. Finally, the issue of missing data in a non-ignorable fashion can be easily addressed through appropriately constructed neighborhoods and similarity (2.4).

2.3.2. Discriminative and separable dictionary learning. We aim to leverage the supervised information (i.e. subjects) of input signals to learn a discriminative and separable dictionary. Assume the available data are organized in a K th-order tensor $\mathbf{X}_n \in \mathbb{R}^{I_1 \times I_2 \times \dots \times I_K}$. According to the sperebale dictionary models [30], given *coordinate dictionaries* $\mathbf{U}^{(k)} \in \mathbb{R}^{I_k \times R_k}$, *coefficient tensors* $\mathbf{G}, \mathbf{H} \in \mathbb{R}^{R_1 \times R_2 \times \dots \times R_K}$, and a *noise tensor* \mathbf{E}_n , we can express $\mathbf{x}_n = \text{vec}(\mathbf{X}_n)$ as

$$(2.18) \quad \mathbf{x}_n = \left(\bigotimes_{n \in [N]} \mathbf{U}^{(n)} \right) (\mathbf{g}_n + \mathbf{h}_n) + \varepsilon_n,$$

where $\mathbf{g}_n = \text{vec}(\mathbf{G}_n)$, $\mathbf{h}_n = \text{vec}(\mathbf{H}_n)$ and $\varepsilon_n = \text{vec}(\mathbf{E}_n)$.

Let

$$I = \prod_{k \in [K]} I_k \quad \text{and} \quad R = \prod_{k \in [K]} R_k.$$

By concatenating N i.i.d. noisy observations $\{\mathbf{x}_n\}_{n=1}^N$ that are realizations from the data generating process posited in (2.18) into $\mathbf{X} \in \mathbb{R}^{I \times N}$, we obtain the following discriminative dictionary learning model

$$(2.19) \quad F(s^h, \mathbf{X}; \mathbf{Z}) + \lambda_1 \|\mathbf{G}\|_1 + \lambda_2 \|\mathbf{H}\|_1 + \lambda_3 \sum_{m=1}^M \sum_{\kappa=1}^{\pi} \|\mathbf{H}_{m_\kappa}\|_F,$$

where $\mathbf{Z} = \mathbf{U}(\mathbf{G} + \mathbf{H})$; $\mathbf{U} = \bigotimes_{k \in [K]} \mathbf{U}^{(k)}$ is the basis matrix; \mathbf{G} and \mathbf{H} are coefficient matrices; and λ_2 and λ_3 are tuning parameters.

Note that in (2.19), we consider a *sparse group lasso* penalty for the structured core \mathcal{H} . We note that this penalty yields solutions that are sparse at both the group and individual feature levels for all subjects $m = 1, 2, \dots, M$ [71].

2.3.3. Image Analytics and Tensor Completion. On many occasions, the available image data set contain multiple shots of the same subject, as is the case in the CMU faces database [70]. As an illustration, using 30 subjects from the data base and extracting 11 poses under 21 lighting conditions, we end up with a tensor comprising of $6930 = 30 \times 11 \times 21$ images, of 32×32 dimension each. Since each subject remains the same under different illuminations for the same pose, and there are also a number of other subjects with the same pose, we consider the following partition of the core tensor \mathcal{H}

$$\mathcal{H}_1 = (1, :, :, :) \mid \mathcal{H}_2 = (2, :, :, :) \mid \dots \mid \mathcal{H}_{30} = (30, :, :, :).$$

Further, if the resulting tensor is missing certain illuminations or poses for selective subjects, a completion task needs to be undertaken. Existing methods use either factorization or completion schemes to recover the missing components. However, as the number of missing entries increases, factorization schemes may overfit the model because of incorrectly predefined ranks, while completion schemes may fail to obtain easy to interpret model factors. To this end, we propose a model that combines a rank minimization technique with DCOT model decomposition. Moreover, as the model structure is implicitly included in the DCOT model, we use the similarity function s^h , to borrow neighborhood information from image data over a image-subject specific network. The proposed method leverages the two proposed schemes and accurately estimates the model factors and missing entries via the following penalized loss function:

$$(2.20) \quad \min_{\mathcal{F}} F(s^h, \mathcal{X}; \mathcal{Z}) + \lambda_1 \|\mathcal{G}\|_F^2 + \lambda_2 \|\mathcal{H}\|_F^2 + \sum_{n=1}^N \lambda_{3,n} \|\mathbf{U}^{(n)}\|_*,$$

where $\mathbf{U}^{(n)} \in \mathbb{R}^{I_n \times I_n}$, \mathcal{G} and $\mathcal{H} \in \mathbb{R}^{I_1 \times I_2 \times \dots \times I_N}$ are the core tensors.

Formulation (2.20) leverages similarity between members of I_3 , i.e, $\mathcal{H}_{m_\kappa} = (1, :, \kappa, :)$ for $\kappa = 1, 2, \dots, \pi$, and across subjects I_1 . The results are briefly depicted in Figure 2.1.

2.3.4. Integrative tensor factorization for Omics multi-modal data. A major challenge for integrative analysis of multi-modal Omics data is the heterogeneity present across samples, as well as across different Omics data sources, which makes it difficult to identify the coordinated signal of interest from source-specific noise or extraneous effects. Matrix and tensor factorization methods are broadly used across multiple domains to analyze genomic datasets represented as matrices [32, 57, 33] and tensors [36, 39, 46, 73, 84], respectively. In contrast to these methods, DCOT provides an approach for jointly decomposing the data matrices as slices of the data tensor. Formally, for non-negative observationally-linked datasets $\mathbf{X}_1, \dots, \mathbf{X}_{I_3}$, we form a 3-way tensor $\mathcal{X} \in \mathbb{R}^{I_1 \times I_2 \times I_3}$. Then, based on a non-negative DCOT factorization, the

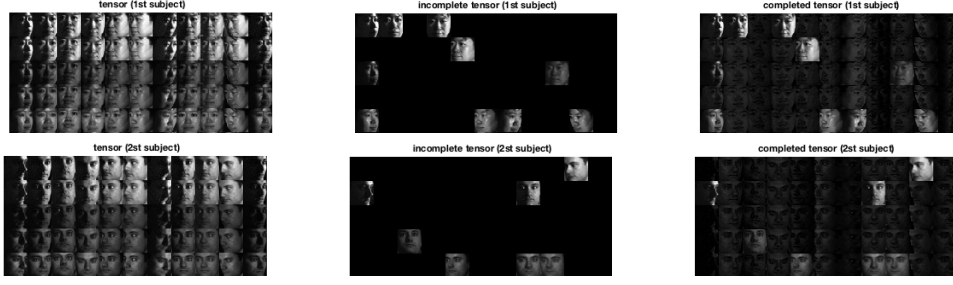


Figure 2.1: Illustration of tensor completion with DCOT (3-th iteration step) on CMU face data set of size $30 \times 11 \times 21 \times 1024$. The last column shows that DCOT encourages joint structures within subgroups of each subject and discriminative structures across members of different subjects.

objective function becomes

$$\min_{\mathcal{J}} F(s^h, \mathcal{X}; \mathcal{Z}) + \lambda_1 \mathbb{1}_{\mathcal{G} \geq 0}(\mathcal{G}) + \lambda_2 \mathbb{1}_{\mathcal{H} \geq 0}(\mathcal{H}) + \sum_{n=1}^N \lambda_{3,n} \mathbb{1}_{\mathbf{U}^{(n)} \geq 0}(\mathbf{U}^{(n)}),$$

where $\mathbb{1}_A(\cdot)$ is the indicator function of set A ; $\mathbf{U}^{(n)} \in \mathbb{R}^{I_n \times R_n}$ is the n -th nonnegative factor matrix for $n = 1, 2$, consisting of latent components; $\mathcal{G} \in \mathbb{R}^{R_1 \times R_2 \times R_3}$ is a core tensor reflecting the connections (or links) between the latent components and is able to capture the homogeneous part across sources; and \mathcal{H} is defined as

$$\mathcal{H}(:, :, 1) = \mathcal{H}(:, :, 2) = \cdots = \mathcal{H}(:, :, I_3),$$

in order to detect coordinated activity (heterogeneous part) across multiple genomic variables in the form of multi-dimensional modules.

3. Optimization. Next, we introduce an optimization algorithm for the DCOT decomposition model, based on a linearized ADMM one. Before presenting the proposed algorithm, we introduce a regularization scheme that overcomes ill-conditioning issues present in many tensor factorizations.

3.1. Orthogonal Total Variation Regularization. An alternating minimization procedure is frequently used in tensor decompositions and is often effective, but it has one significant drawback, namely, that the condition number of the coefficient matrices is the square of the condition number of $(\mathbf{G}_{(n)} + \mathbf{H}_{(n)}) (\bigotimes_{k \neq n} \mathbf{U}^{(k)})^\top$. When $(\mathbf{G}_{(n)} + \mathbf{H}_{(n)}) (\bigotimes_{k \neq n} \mathbf{U}^{(k)})^\top$ is ill conditioned, alternating minimization procedures become slow to converge and may even break down. For example, the convergence rate of the gradient descent method for solving (2.3) heavily depends on the condition number of $(\mathbf{G}_{(n)} + \mathbf{H}_{(n)}) (\bigotimes_{k \neq n} \mathbf{U}^{(k)})^\top$. For higher values of this condition number, the contours of the quadratic objective function become more elongated, the corresponding “zig-zagging” behavior of the algorithm becomes more pronounced, which in turn implies degraded convergence behavior. Hence, it is easy to observe that, for ill-conditioned $\mathbf{U}^{(n)}$, the corresponding tensor factorization subproblems become ill-conditioned

in every iteration as well, unless we “force” the sequence of estimates $\mathbf{U}^{(n)}$ to converge to a better conditional $\hat{\mathbf{U}}^{(n)}$.

On the other hand, in most tensor decomposition models the factor matrices are required to be orthogonal. However, it is generally difficult to solve problem (2.3) since the orthogonality constraints can lead to local minima, while on several occasions the corresponding subproblems are NP-hard [87]. Even generating a sequence of feasible points is not easy, since preserving the orthogonality constraints can be numerically expensive. Most existing constraint-preserving algorithms use matrix re-orthogonalization which requires matrix factorizations obtained from singular value decompositions [40].

Hence, the challenge becomes to design an approach that the aforementioned properties. To achieve these goals, we propose an alternative solution, called *Orthogonal Total Variation* (OTV) regularization which has a simple implementation and results in accelerating tensor decomposition problems.

Let $\mathbf{A} = [\mathbf{a}]_n$ and $\mathbf{B} = [\mathbf{b}]_m$ be square matrices of dimension n and m , respectively. The *Kronecker minus* of \mathbf{A} and \mathbf{B} denoted by $\mathbf{A} \ominus \mathbf{B}$ is defined as:

$$(3.1) \quad \mathbf{A} \ominus \mathbf{B} = (\mathbf{A} \otimes \mathbf{I}_m) - (\mathbf{I}_n \otimes \mathbf{B}),$$

where \otimes denotes the Kronecker product and \mathbf{I}_m and \mathbf{I}_n are identity matrices of order m and n , respectively. For example, the Kronecker minus of two 2×2 matrices $\mathbf{A} = [\mathbf{a}]_n$ and $\mathbf{B} = [\mathbf{b}]_m$ is given by

$$\mathbf{A} \ominus \mathbf{B} = \begin{bmatrix} \mathbf{a}_{11} - \mathbf{b}_{11} & \mathbf{b}_{12} & \mathbf{a}_{12} & 0 \\ \mathbf{b}_{21} & \mathbf{a}_{22} - \mathbf{b}_{22} & 0 & \mathbf{a}_{12} \\ \mathbf{a}_{21} & 0 & \mathbf{a}_{22} - \mathbf{b}_{11} & \mathbf{b}_{12} \\ 0 & \mathbf{a}_{21} & \mathbf{b}_{21} & \mathbf{a}_{22} - \mathbf{b}_{22} \end{bmatrix}.$$

Definition 3.1. For a sequence of factor matrices $\mathbf{U}^{(i)} \in \mathbb{R}^{I_i \times R_i}$, $i = 1, \dots, N$, in the DCOT decomposition $\mathbf{Z} = (\mathcal{G} + \mathcal{H}) \times_1 \mathbf{U}^{(1)} \times_2 \mathbf{U}^{(2)} \times_3 \dots \times_N \mathbf{U}^{(N)}$, we define the orthogonal total variation regularizer as follows:

$$(3.2) \quad J_3^{otv}(\mathbf{U}) := \sum_{i=1}^{N-1} v_{i,i+1}(\mathbf{U}^{(i)}, \mathbf{U}^{(i+1)}),$$

where

$$v_{i,i+1}(\mathbf{U}^{(i)}, \mathbf{U}^{(i+1)}) = \mu^{(i)} \|\mathbf{U}^{(i)\top} \mathbf{U}^{(i)} \ominus \mathbf{U}^{(i+1)\top} \mathbf{U}^{(i+1)}\|_F^2,$$

and $\mu^{(i)}$ correspond to non-negative weights and \ominus is as in (3.1). A simple, but effective strategy is to set the weights to $\mu^{(1)} = \dots = \mu^{(N)} = \frac{1}{N^2}$.

Note that the reason of using \ominus instead of $-$ operation is that ranks R_1, \dots, R_N are not equal. Otherwise, one can simply use the standard $-$ operation. Some examples of v include the Frobenius norm and sum of the element-wise smooth functions (of the form $v(\mathbf{X}) = \sum_{i,j} v_{ij}(\mathbf{X}_{ij})$) with the optimum at zero.

3.2. A linearized ADMM method for penalized DCOT factorization. In this section, a *multi-block linearized* ADMM is developed to solve the regularized DCOT decomposition problem posited in (2.3).

To obtain the updates in the standard ADMM, we first formulate (2.3) as follows:

$$(3.3) \quad \begin{aligned} & \underset{\mathbf{Z}, \mathcal{H}, \mathcal{G}, \mathbf{U}}{\text{minimize}} && F(s^h, \mathbf{X}; \mathbf{Z}) + \lambda_1 J_1(\mathcal{G}) + \lambda_2 J_2(\mathcal{H}) + \lambda_3 J_3(\mathbf{U}), \\ & \text{s.t.} && (\mathcal{G} + \mathcal{H}) \times_1 \mathbf{U}^{(1)} \cdots \times_N \mathbf{U}^{(N)} - \mathbf{Z} = 0. \end{aligned}$$

The importance of this formulation is that the gradient of a smooth function w.r.t \mathbf{Z} can be calculated via a standard vector operation, allowing us to take advantage of existing good implementations for DCOT decomposition.

Note that problem (3.3) is non-convex; hence, global convergence is a priori not guaranteed. Recent work [35, 48, 74] studied the convergence of ADMM for non-convex and non-smooth problems under linear constraints. However, the constraints in the tensor factorization problem are not linear. To avoid introducing auxiliary variables and still solve (3.4) efficiently, we propose to approximate (3.4) by linearizing the smooth terms with respect to the factor matrices and core tensors. With this linearization, the resulting approximation to (3.4) is then simple enough to have a closed form solution and we are able to provide the global convergence under mild conditions ².

By introducing the dual variable \mathbf{Y} and dual parameter $\gamma > 0$, the standard ADMM is constructed for an augmented Lagrangian function defined by

$$(3.4) \quad \begin{aligned} \mathcal{L}(\mathcal{T}) = & F(s^h, \mathbf{X}; \mathbf{Z}) + \lambda_1 J_1(\mathcal{G}) + \lambda_2 J_2(\mathcal{H}) + \lambda_3 J_3(\mathbf{U}) \\ & - \langle \mathbf{Y}, (\mathcal{G} + \mathcal{H}) \times_1 \mathbf{U}^{(1)} \cdots \times_N \mathbf{U}^{(N)} - \mathbf{Z} \rangle \\ & + \frac{\gamma}{2} \|(\mathcal{G} + \mathcal{H}) \times_1 \mathbf{U}^{(1)} \cdots \times_N \mathbf{U}^{(N)} - \mathbf{Z}\|_F^2, \end{aligned}$$

where $\mathcal{T} := (\mathbf{U}^{(1)}, \dots, \mathbf{U}^{(N)}, \mathcal{G}, \mathcal{H}, \mathbf{Z}, \mathbf{Y})$ contains the model parameters.

²It is also worth mentioning that we have implemented and tested other local decent algorithms, such as accelerated block coordinate descent [91] for solving various DCOT decomposition problems, including the recovery of missing images from incomplete tensors. Although the latter method converges faster than the proposed algorithm, the linearized ADMM (Algorithm 3.1) demonstrates superior performance in the quality of the obtained solution.

In a typical iteration of the ADMM for solving (3.3), the following updates are implemented:

$$\begin{aligned}
\mathbf{U}_{k+1}^{(1)} &= \underset{\mathbf{U}^{(1)}}{\operatorname{argmin}} \quad \mathcal{L}(\underbrace{\mathbf{U}^{(1)}, \mathbf{U}_k^{(2)}, \dots, \mathbf{U}_k^{(N)}}_{:=\mathcal{T}_k^{\mathbf{U}^{(1)}}}, \mathcal{G}_k, \mathcal{H}_k, \mathbf{Z}_k, \mathbf{Y}_k), \\
\mathbf{U}_{k+1}^{(n)} &= \underset{\mathbf{U}^{(n)}}{\operatorname{argmin}} \quad \mathcal{L}(\underbrace{\mathbf{U}_{k+1}^{(1)}, \dots, \mathbf{U}_{k+1}^{(n-1)}, \mathbf{U}^{(n)}, \mathbf{U}_k^{n+1}, \dots, \mathbf{U}_k^{(N)}}_{:=\mathcal{T}_k^{\mathbf{U}^{(n)}}}, \mathcal{G}_k, \mathcal{H}_k, \mathbf{Z}_k, \mathbf{Y}_k), \\
\mathbf{U}_{k+1}^{(N)} &= \underset{\mathbf{U}^{(N)}}{\operatorname{argmin}} \quad \mathcal{L}(\underbrace{\mathbf{U}_{k+1}^{(1)}, \mathbf{U}_{k+1}^{(2)}, \dots, \mathbf{U}_{k+1}^{(N-1)}, \mathbf{U}^{(N)}}_{:=\mathcal{T}_k^{\mathbf{U}^{(N)}}}, \mathcal{G}_k, \mathcal{H}_k, \mathbf{Z}_k, \mathbf{Y}_k), \\
\mathcal{G}_{k+1} &= \underset{\mathcal{G}}{\operatorname{argmin}} \quad \mathcal{L}(\underbrace{\mathbf{U}_{k+1}^{(1)}, \dots, \mathbf{U}_{k+1}^{(N)}}_{:=\mathcal{T}_k^{\mathcal{G}}}, \mathcal{G}, \mathcal{H}_k, \mathbf{Z}_k, \mathbf{Y}_k), \\
\mathcal{H}_{k+1} &= \underset{\mathcal{H}}{\operatorname{argmin}} \quad \mathcal{L}(\underbrace{\mathbf{U}_{k+1}^{(1)}, \dots, \mathbf{U}_{k+1}^{(N)}, \mathcal{G}_{k+1}}_{:=\mathcal{T}_k^{\mathcal{H}}}, \mathcal{H}, \mathbf{Z}_k, \mathbf{Y}_k), \\
\mathbf{Z}_{k+1} &= \underset{\mathbf{Z}}{\operatorname{argmin}} \quad \mathcal{L}(\underbrace{\mathbf{U}_{k+1}^{(1)}, \dots, \mathbf{U}_{k+1}^{(N)}, \mathcal{G}_{k+1}, \mathcal{H}_{k+1}}_{:=\mathcal{T}_k^{\mathbf{Z}}}, \mathbf{Z}, \mathbf{Y}_k), \\
(3.5) \quad \mathbf{Y}_{k+1} &= \mathbf{Y}_k - \gamma((\mathcal{G}_{k+1} + \mathcal{H}_{k+1}) \times_1 \mathbf{U}_{k+1}^{(1)} \cdots \times_N \mathbf{U}_{k+1}^{(N)} - \mathbf{Z}_{k+1}),
\end{aligned}$$

where $n \in \{2, 3, \dots, N-1\}$.

As previously mentioned, problem (3.3) is non-convex and thus global convergence is not a priori guaranteed. To address this issue, we first regularize each subproblem of (3.4) w.r.t $\mathcal{G}, \mathcal{H}, \mathbf{U}^{(1)}, \dots, \mathbf{U}^{(N)}$, and consider the following updates in ADMM:

$$(3.6) \quad \mathbf{U}_{k+1}^{(n)} = \underset{\mathbf{U}^{(n)}}{\operatorname{argmin}} \quad \mathcal{L}(\mathcal{T}_k^{\mathbf{U}^{(n)}}) + \frac{\varrho^n}{2} \|\mathbf{U}^{(n)} - \mathbf{U}_k^{(n)}\|_F^2, \quad n = 1, \dots, N,$$

$$(3.7) \quad \mathcal{G}_{k+1} = \underset{\mathcal{G}}{\operatorname{argmin}} \quad \mathcal{L}(\mathcal{T}_k^{\mathcal{G}}) + \frac{\varrho^g}{2} \|\mathcal{G} - \mathcal{G}_k\|_F^2,$$

$$(3.8) \quad \mathcal{H}_{k+1} = \underset{\mathcal{H}}{\operatorname{argmin}} \quad \mathcal{L}(\mathcal{T}_k^{\mathcal{H}}) + \frac{\varrho^h}{2} \|\mathcal{H} - \mathcal{H}_k\|_F^2,$$

$$(3.9) \quad \mathbf{Z}_{k+1} = \underset{\mathbf{Z}}{\operatorname{argmin}} \quad \mathcal{L}(\mathcal{T}_k^{\mathbf{Z}}),$$

$$(3.10) \quad \mathbf{Y}_{k+1} = \mathbf{Y}_k - \gamma((\mathcal{G}_{k+1} + \mathcal{H}_{k+1}) \times_1 \mathbf{U}_{k+1}^{(1)} \cdots \times_N \mathbf{U}_{k+1}^{(N)} - \mathbf{Z}_{k+1}),$$

where positive constants ϱ^g , ϱ^h , and $\{\varrho^n\}_{n=1}^N$ are regularization parameters.

To avoid introducing auxiliary variables and still solve large-scale instances of subproblems (3.6)-(3.8) efficiently, we propose to approximate these sub-problems by *linearizing* the function

$$(3.11) \quad \bar{\mathcal{L}}(\mathcal{T}) := \frac{\gamma}{2} \|(\mathcal{G} + \mathcal{H}) \times_1 \mathbf{U}^{(1)} \cdots \times_N \mathbf{U}^{(N)} - \mathbf{Z} - \frac{1}{\gamma} \mathbf{Y}\|_F,$$

Algorithm 3.1 Regularized and smooth DCOT factorization via linearized ADMM.

1: Input:

- data tensor $\mathcal{X} \in \mathbb{R}^{I_1 \times I_2 \times \dots \times I_N}$;
- regularization parameters $\lambda_1, \lambda_2, \lambda_3 > 0$;
- a smoothing parameter h ;
- a dual step size $\gamma > 2L$.

2: Initialize:

- $k = 0$;
- factor matrices $\{\mathbf{U}_k^{(n)}\}_{n=1}^N = \text{rand}(R_n, I_n)$;
- $\mathcal{Z}_k = \mathcal{X}$ and tensor cores $\mathcal{G}_k = \mathcal{H}_k = \mathcal{X} \times_1 \mathbf{U}_k^{(1)} \times_2 \mathbf{U}_k^{(2)} \dots \times_N \mathbf{U}_k^{(N)}$;
- dual variable $\mathcal{Y}_k = \text{zeros}(I_1, I_2, \dots, I_N)$;
- smoothing function s^h by using (2.4).

3: Iterate until the stopping criterion is met:

- update \mathbf{U}_{k+1} as per Appendix .0.1;
 - update \mathcal{G}_{k+1} as per Appendix .0.2;
 - update \mathcal{H}_{k+1} as per Appendix .0.3;
 - update \mathcal{Z}_{k+1} as per Appendix .0.4;
 - $\mathcal{Y}_{k+1} = \mathcal{Y}_k - \gamma([\mathcal{G}_{k+1}, \mathcal{H}_{k+1}; \mathbf{U}_{k+1}] - \mathcal{Z}_{k+1})$;
 - $k = k + 1$.
-

w.r.t $\mathbf{U}^{(1)}, \dots, \mathbf{U}^{(N)}, \mathcal{G}, \mathcal{H}$ as follows

$$(3.12) \quad \mathbf{U}_{k+1}^{(n)} = \underset{\mathbf{U}^{(n)}}{\operatorname{argmin}} \langle \nabla_{\mathbf{U}^{(n)}} \bar{\mathcal{L}}(\mathcal{T}_k^{\mathbf{U}_k^{(n)}}), \mathbf{U}^{(n)} - \mathbf{U}_k^{(n)} \rangle + \lambda_3 J_3(\mathbf{U}) + \frac{\varrho^n}{2} \|\mathbf{U}^{(n)} - \mathbf{U}_k^{(n)}\|_F^2,$$

$$(3.13) \quad \mathcal{G}_{k+1} = \underset{\mathcal{G}}{\operatorname{argmin}} \langle \nabla_{\mathcal{G}} \bar{\mathcal{L}}(\mathcal{T}_k^{\mathcal{G}_k}), \mathcal{G} - \mathcal{G}_k \rangle + \lambda_1 J_1(\mathcal{G}) + \frac{\varrho^g}{2} \|\mathcal{G} - \mathcal{G}_k\|_F^2,$$

$$(3.14) \quad \mathcal{H}_{k+1} = \underset{\mathcal{H}}{\operatorname{argmin}} \langle \nabla_{\mathcal{H}} \bar{\mathcal{L}}(\mathcal{T}_k^{\mathcal{H}_k}), \mathcal{H} - \mathcal{H}_k \rangle + \lambda_2 J_2(\mathcal{H}) + \frac{\varrho^h}{2} \|\mathcal{H} - \mathcal{H}_k\|_F^2,$$

where $\nabla_{\mathbf{U}^{(n)}} \bar{\mathcal{L}}(\cdot)$, $\nabla_{\mathcal{G}} \bar{\mathcal{L}}(\cdot)$, and $\nabla_{\mathcal{H}} \bar{\mathcal{L}}(\cdot)$ denote the gradients of (3.11) w.r.t. $\mathbf{U}^{(n)}$, \mathcal{G} and \mathcal{H} , respectively.

Next, we establish the global convergence of the standard multi-block ADMM for solving the DCOT decomposition problem, by using the Kurdyka-Lojasiewicz property of the objective function in (3.4).

Theorem 3.2 (global convergence). *Suppose Assumption 2.2 holds and $\mathcal{L}(\mathcal{T})$ is a Kurdyka-Lojasiewicz function. Then, the sequence $\mathcal{T}_k = (\mathbf{U}_k^{(1)}, \dots, \mathbf{U}_k^{(N)}, \mathcal{G}_k, \mathcal{H}_k, \mathcal{Z}_k, \mathcal{Y}_k)$ generated by Algorithm 3.1 from any starting point converges to a critical point of problem (3.4).*

It is worth mentioning that $\mathcal{L}(\mathcal{T})$ will be a Kurdyka-Lojasiewicz function if the loss function F , and the penalty functions $\{J_1(\cdot), J_2(\cdot), J_{3,1}(\cdot), J_{3,2}(\cdot), \dots, J_{3,N}(\cdot)\}$ satisfy growth condition, or uniform convexity or they are general convex semi-algebraic or real analytic functions; see, [14] for more information.

4. Consistency of the DCOT factorization. This section presents theoretical properties to quantify the asymptotic behavior of the proposed DCOT factorization using the smoothing loss function defined in (2.9). In particular, we provide the estimation error rate as a function of the sample size Ω and tuning parameter λ and show the necessity of the smoothing function s^h for providing faster convergence rate and small prediction error. To do so, let $\hat{\mathbf{Z}} \in \Gamma(\mathbf{Z})$ denotes an estimator of \mathbf{Z}^* , the prediction accuracy of $\hat{\mathbf{Z}}$ is defined by the root mean square error (RMSE):

$$(4.1) \quad \rho(\hat{\mathbf{Z}}, \mathbf{Z}^*) = \left\{ \frac{1}{\Omega} \sum_{i_1 \dots i_N \in \Omega} (\hat{z}_{i_1 \dots i_N} - z_{i_1 \dots i_N}^*)^2 \right\}^{\frac{1}{2}}.$$

In order to provide the asymptotic behavior of penalized DCOT, we require the following technical assumptions

Assumption 4.1. Let c_{i_n, j_n} be the label constraints defined in (2.4). Then, there exist constants $a_1 \geq 0$ and $\alpha > 0$ such that for any N -tuples (i_1, i_2, \dots, i_N) and (j_1, j_2, \dots, j_N)

$$|z_{i_1 \dots i_N}^* - z_{j_1 j_2 \dots j_N}^*| \leq a_1 R_{\min} \max \left\{ \left(\prod_{n=1}^N d(\mathbf{y}_{i_n}, \mathbf{y}_{j_n}) \right)^\alpha, \mathbb{1}_{\prod_{n=1}^N c_{i_n, j_n} = 0} \right\},$$

where $d(\mathbf{y}_{i_n}, \mathbf{y}_{j_n})$ denotes the distance between \mathbf{y}_{i_n} and \mathbf{y}_{j_n} and $R_{\min} = \min\{R_1, R_2, \dots, R_N\}$. The corresponding expression in the maximum operator is set as 0 if \mathbf{y}_{i_n} or c_{i_n, j_n} is absent for $n \in [N]$.

Assumption 4.1 provides the smoothness of $z_{i_1 \dots i_N}^*$ in terms of the side information \mathbf{y} and is widely used in literature [82, 85, 8]. This assumption is mild when for example all \mathbf{y}_{i_n} are available, and is relatively more restrictive when they are absent.

Assumption 4.2. For a window size $h > 0$ and positive constants α and β , the similarity function s^h defined in (2.4) satisfies

- A1. $\sum_{j_1 \dots j_N} s_{i_1 \dots i_N, j_1 \dots j_N}^h = 1$;
- A2. $\max_{i_1 \dots i_N} \sum_{j_1, \dots, j_N \in \Omega} (s_{i_1 \dots i_N, j_1 \dots j_N}^h)^2 \leq (|\Omega| h^\beta)^{-1}$;
- A3. $\max_{i_1 \dots i_N} \sum_{j_1, \dots, j_N \in \Omega} s_{i_1 \dots i_N, j_1 j_2 \dots j_N}^h (\prod_{n=1}^N d(\mathbf{y}_{i_n}, \mathbf{y}_{j_n}))^\alpha \leq h^\alpha$;

Assumption 4.2 is a standard assumption for smoothing kernels such as the Gaussian one. Indeed, the choice of kernels should match up the smoothness at an order α of $z_{i_1 \dots i_N}^*$ [66].

The next result provides a general upper bound of the root mean square error $\rho(\hat{\mathbf{Z}}, \mathbf{Z}^*)$, which may vary by the window size h , minimum rank of the data tensor R_{\min} , and the number of observed variables Ω .

Theorem 4.3. Suppose Assumptions 4.1 and 4.2 hold. Then, for some positive constant a_2 , we have

$$P(\rho(\hat{\mathbf{Z}}, \mathbf{Z}^*) \geq \eta) \leq \exp(-a_2 \eta^2 |\Omega| h^\beta + \sum_{n \in [N]} \log I_n),$$

provided that

$$\eta \geq \max\{\sqrt{R_{\min}} h^\alpha, (\Omega h^\beta)^{-1/2}\} \sum_{n \in [N]} \log I_n \quad \text{and} \quad \lambda J(\mathbf{Z}^*) \leq \eta^2.$$

The convergence rate of DCOT factorization for specific window size h then becomes

$$\max\{\sqrt{R_{\min}}h^\alpha, (\Omega h^\beta)^{-1/2}\} \sum_{n \in [N]} \log I_n.$$

Further, if $\beta = 1$, $h = (R_{\min}|\Omega|)^{\frac{-1}{2\alpha+1}}$ and $R_{\min} = O(1)$, then the convergence rate of DCOT is

$$(4.2) \quad O\left(\frac{\sum_{n \in [N]} \log I_n}{|\Omega|^{\frac{\alpha}{2\alpha+1}}}\right).$$

5. Experimental results. We test the performance of DCOT and its smoothing version (called S-DCOT) on a number of data analytics tasks, including subspace clustering, imaging tensor completion and denoising, recommender systems, dictionary learning and multiplatform cancer analysis in terms of accuracy and scalability.

Algorithm 3.1 requires a good initializer to achieve good performance, which is also the case for the Tucker decomposition. To that end, we use DCOT with HOSVD [22] and random initialization, called DCOT(H) and DCOT(R), respectively. Without knowledge of the tensor rank, DCOT gains no advantage from using the random or HOSVD initialization, hence, we use the identity initialization for factor matrices (-called DCOT(I)). The variants of DCOT based on different initializations used in our experimental work are summarized next:

- DCOT(R): DCOT factorization with random initialization, i.e. $\mathbf{U}^{(n)} = \text{rand}(R_n, I_n)$;
- DCOT(H): DCOT factorization with HOSVD initialization. In this setting, given a tensor \mathcal{X}_0 , we construct the mode-“n” matricization $\mathcal{X}_{0,(n)}$. Then, we compute the singular value decomposition $\mathcal{X}_{0,(n)} = \mathbf{U}_r^{(n)} \mathbf{D}_r^{(n)} \mathbf{V}_r^{(n)}$, and store the left singular vectors $\mathbf{U}^{(n)}$;
- DCOT(I): DCOT factorization with identity initialization for factor matrices, i.e. $\mathbf{U}^{(n)} = \text{eye}(I_n, I_n)$.

In all of these approaches, the core tensor \mathcal{G} is the projection of \mathcal{X} onto the tensor basis formed by the factor matrices $\{\mathbf{U}^{(n)}\}_{n=1}^N$, i.e., $\mathcal{G} = \mathcal{X} \times_{n=1}^N \mathbf{U}^{(n)\top}$. The initial heterogeneous core \mathcal{H} is set to \mathcal{G} . For solving the optimization problem (3.9), we use limited-memory BFGS with bound constraints (L-BFGS-B) [15, 76].

5.1. DCOT for tensor completion problems. Next, we examine the performance of DCOT factorization for different tensor completion tasks.

5.1.1. Image completion and denoising problems. We use S-DCOT for image completion and compare it with the following tensor factorization methods for image processing: fully Bayesian CP factorization using mixture prior (FBCP-MP) [96], simultaneous tensor decomposition and completion (STDC) using factor prior [19], high accuracy low rank tensor completion (HaLRTC) [51], exact tensor completion using TSVD [94], and Low-rank Tensor Completion by Parallel Matrix Factorization (TMAC) [90]³.

³The codes can be obtained from <https://github.com/qbzha0/BCPF>, <https://sites.google.com/site/fallcolor/projects/stdc>, <http://www.cs.rochester.edu/u/jliu/> and <https://xu-yangyang.github.io/software.html>, respectively.

We applied our tensor completion method proposed in Subsection 2.3.3 to the 4D CMU faces database [70] and the Cine Cardiac data set [49]. The CMU data set [70] comprises of 65 subjects with 11 poses, and 21 types of illumination. All face images are aligned by their eye coordinates and then cropped and resized into 32×32 images. Images are vectorized, and the data set is arranged as a fourth-order tensor. Thus, the size of the CMU data is $(65 \times 11 \times 21 \times 1024)$. Since each facial image is similar under different illuminations, but for similar faces, poses are not necessarily similar, we consider the following partitions

$$\mathcal{H}_{m_\kappa} = \mathcal{H}(m, :, \kappa, :), \quad \kappa = 1, \dots, 21, \quad m = 1, \dots, 65, \quad \text{CMU dataset},$$

which enforces the similarity across members of I_3 .

Dynamic cardiac imaging is performed either in cine or real-time mode. Cine MRI, the clinical gold-standard for measuring cardiac function/volumetrics [12], produces a movie of roughly 20 cardiac phases over a single cardiac cycle (heart beat). However, by exploiting the semi-periodic nature of cardiac motion, it is actually formed over many heart beats. Cine sampling is gated to a patients heart beat, and as each data measurement is captured it is associated with a particular cardiac phase. This process continues until enough data has been collected such that all image frames are complete. Typically, an entire 2D cine cardiac MRI series is acquired within a single breath hold (less than 30 secs). In our experiment, we consider a bSSFP long-axis cine sequence ($n = 192, t = 19$) acquired at 1.5 T (Tesla) magnets, using an phased-array cardiac receiver coil ($l = 8$ channels) [16]. Hence, the size of the Cine Cardiac data is $(192 \times 192 \times 8 \times 19)$. We use the following partitions

$$\mathcal{H}_{m_\kappa} = \mathcal{H}(:, :, m, \kappa), \quad \kappa = 1, \dots, 19, \quad m = 1, \dots, 8, \quad \text{Cine Cardiac dataset},$$

which enforces the similarity across time dimension.

We control the tradeoff in (3.4) between the data tensor term and the low rank tensor as follows:

$$(5.1) \quad \lambda_1 = \frac{10}{\|\mathcal{X}\|_F^2}, \quad \lambda_2 = 0.01\lambda_1, \quad \lambda_{3,i} = 5 \quad \text{for } i = 1, \dots, 4, \quad \gamma = \frac{10}{\sigma_1(\mathbf{X}_{(1)}\mathbf{X}_{(1)}^\top)},$$

where σ_1 denotes the largest singular value of a matrix.

As shown in [19, Section 3.1.1], the images should lie on joint sub-manifolds. Hence, to define a label function $c_{i_n, j_n} \in \{0, 1\}$ for each (i_n, j_n) pair, we connect i_n th face image with its nearest neighbor indices (we use the 2-nearest-neighbor function (2-NN)). We also measure the average Euclidean distance between two subject groups and then determine if they are 2-NN. For the proposed S-DCOT, the tensor similarities are set to $s_{i_1 \dots i_N, j_1 \dots j_N}^h = c_{i_1, j_1} c_{i_2, j_2} \dots c_{i_N, j_N}$.

Table 5.1 shows the completion results on the three imaging data sets. For each given ratio ρ , 5 test runs were conducted and the average relative square error (RSE), $\|\mathcal{X} - \hat{\mathcal{X}}\|/\|\mathcal{X}\|_F$ is used to evaluate the performance. Table 5.1 shows that S-DCOT significantly outperform their competitors.

5.1.2. Rainfall in India. We consider monthly rainfall data for different regions in India for the period 1901–2015, available from Kaggle⁴. For each of 36 regions, 12 months and 115

⁴<https://www.kaggle.com/rajanand/rainfall-in-india>

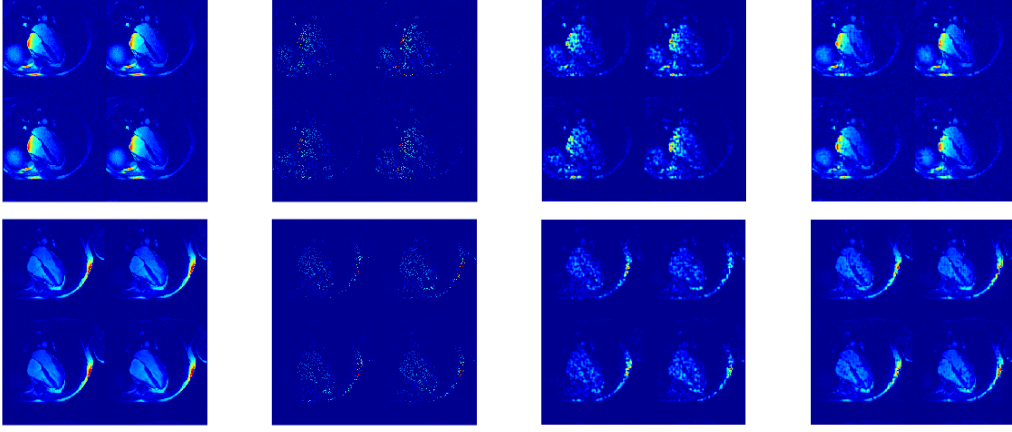


Figure 5.1: Tucker (third column) and DCOT (fourth column) completion results for a cine cardiac MRI series ($192 \times 192 \times 8 \times 19$) with 85% missing rate. The effect of using the supervised core is demonstrated (four images per channel). First and second rows show some images from the channels one and two, respectively. The last column shows S-DCOT outperforms the Tucker-based completion.

Table 5.1: The relative square error (RSE) and runtime (seconds) of tensor completion methods on imaging datasets.

Data	ρ	S-DCOT(I)		FBCP-MP		STDC		HaLRTC		TSVD		TMAC	
		RSE	Time	RSE	Time	RSE	Time	RSE	Time	RSE	time	RSE	Time
CMU	0.8	13.16e-2	44.15	30.28e-2	125.19	21.77e-2	79.48	31.89e-2	225.15	40.11e-2	112.48	29.19e-2	40.69
	0.85	19.26e-2	33.41	38.49e-2	108.23	28.28e-2	57.19	35.14e-2	189.05	43.12e-2	99.82	24.15e-2	39.18
	0.9	22.25e-2	21.10	44.15e-2	97.37	43.21e-2	35.72	49.17e-2	155.28	56.71e-2	104.33	44.26e-2	27.04
	0.95	45.71e-2	22.13	76.41e-2	88.19	81.85e-2	13.11	67.77e-2	114.36	88.79e-2	111.49	85.14e-2	95.6
Cine	0.8	15.12e-2	39.24	42.31e-2	112.39	33.71e-2	88.39	41.11e-2	178.38	49.71e-2	110.13	33.12e-2	55.01
	0.85	20.33e-2	33.17	48.25e-2	110.18	44.15e-2	76.32	55.10e-2	144.82	55.19e-2	114.23	35.11e-2	47.33
	0.9	31.23e-2	31.29	30.24e-2	108.34	55.38e-2	88.72	55.19e-2	107.71	59.13e-2	101.41	46.13e-2	41.55
	0.95	49.44e-2	29.13	77.25e-2	76.85	78.31e-2	23.05	78.08e-2	99.12	76.44e-2	78.45	57.14e-2	39.01

years, we have the total rainfall in millimeters. Since the monthly rainfall is similar within the time periods Jan-Feb, Mar-May, Jun-Sep and Oct-Dec, we consider the following partitions

$$\begin{aligned}
\mathcal{H}(m, 1, :) &= \mathcal{H}(m, 2, :), \\
\mathcal{H}(m, 3, :) &= \mathcal{H}(m, 4, :) = \mathcal{H}(m, 5, :), \\
\mathcal{H}(m, 6, :) &= \mathcal{H}(m, 7, :) = \mathcal{H}(m, 8, :), \\
\mathcal{H}(m, 9, :) &= \mathcal{H}(m, 10, :) = \mathcal{H}(m, 11, :) = \mathcal{H}(m, 12, :), \quad m = 1, 2, \dots, 36,
\end{aligned}$$

which enforces similarity across members of $I_2 = 12$.

We note that \mathcal{H} is a tensor of size $36 \times 12 \times 115$. Label functions c_{i_n, j_n} are defined similar to the previous section. We use a Gaussian kernel with window size h , as the median distance

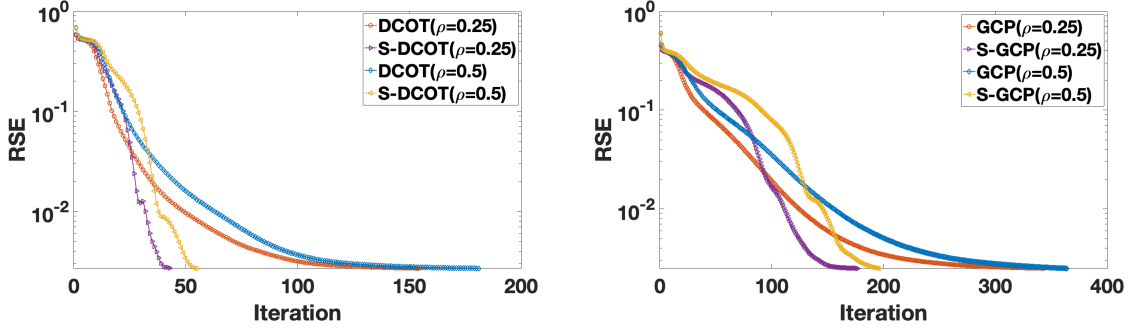


Figure 5.2: Relative squared error (RSE) and the number of iterations of generalized tensor methods on rainfall dataset. **Left:** DCOT vs S-DCOT **Right:** GCP vs S-GCP.

among all fibers to define s_{i_n, j_n}^h . The choice of a Gaussian kernel is due to the better empirical performance obtained, compared to other possibilities. The smoothing functions are normalized such that $\sum_{j_1 \dots j_N} s_{i_1 \dots i_N, j_1 \dots j_N}^h = 1$.

There are several distributions for Rainfall data. As mentioned previously, one option is to assume a Gaussian distribution but impose a nonnegativity constraint. Recently, Hong et. al [34] showed that Gamma distribution is potentially a reasonable model for this dataset. Hence, we investigate the performance of DCOT with smoothing loss (2.16) applied to Rainfall dataset and compare it with the generalized CP (GCP) [34]. We run each method with 5 different random starting points and the average RSE is reported. Figure 5.2 indicates that the proposed S-DCOT has the best performance in terms of both RSE and number of iterations.

5.1.3. DCOT applied to Sparse Count Crime Data. Next, we examine the performance of smooth DCOT factorization for completion and factorization of count datasets. To do so, we consider a real-world crime statistics dataset containing more than 15 years of crime data from the city of Chicago. The data⁵ is organized as a 4-way tensor and obtained from FROSTT [65]. The tensor modes correspond to 6,186 days from 2001 to 2017, 24 hours per day, 77 communities and 32 types of crimes ($6,186 \times 24 \times 77 \times 32$). Each $\mathcal{X}(i_1, i_2, i_3, :)$ is the number of times that a crime occurred in neighborhood i_3 during hour i_2 on day i_1 .

We apply the following partitions

$$\mathcal{H}_{m_\kappa} = \mathcal{H}(:, m, \kappa, :), \quad \kappa = 1, \dots, R_3, \quad m = 1, \dots, R_1, \quad \text{Count Crime dataset,}$$

which enforces the similarity across members of same communities.

We use DCOT with the proposed smoothing Poisson loss function, i.e., (2.14) and nonnegativity constraints. We compare DCOT with GCP [34] with default settings. We run each method with 5 different random starting points and the average RSE is reported. Tensor ranks are set to $R_i = 10$ for $i = 1, \dots, 4$. The ADMM parameters and smoothing functions are chosen similarly to those used in the previous section.

⁵www.cityofchicago.org

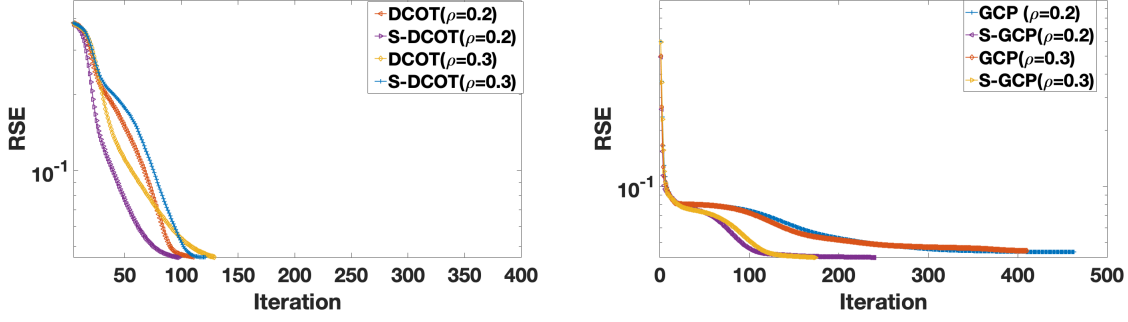


Figure 5.3: The relative square error (RSE) and the number of iterations of generalized tensor methods on count crime dataset. **Left:** DCOT vs S-DCOT **Right:** GCP vs S-GCP.

The results are provided in Figure 5.3. The GCP and S-GCP methods descend much more quickly, but do not reduce the loss quite as much, though this failure to achieve the same final minima is likely an artifact of the function estimation. On the other hand, Figure 5.3 indicates that the proposed S-DCOT has the best performance in terms of RSE. The RSE of the proposed method is less than that of S-GCP, illustrating that S-DCOT has better performance among the competing tensor factorization methods.

5.2. DCOT applied to multi-platform genomic data. DCOT and S-DCOT models have been applied to to understand latent relationships between patients and genes for multi-platform genomic data.

We use the PanCan12 dataset [86] and the Hallmark gene sets collections from MSigDB [47] for obtaining the input tensor and label functions c_{i_n, j_n} , respectively. The PanCan12 contains multi-platform data with mapped clinical information of patient groups into cohorts of twelve cancer typse. The five platforms types used are miRNA-seq (MIR), methylation (MET), somatic mutation (MUT), gene expression (GEX) and copy number variation (CNV).

The PanCan12 dataset was downloaded from the Sage Bionetworks repository, Synapse [59] and was transformed to a 3-order tensor ($4555 \times 15351 \times 5$), containing 4555 sample, 14351 gene and 5 platform. The data for each platform was min-max normalized and was further normalized such that the Frobenius norm became one. In order to efficiently fuse the date into the interpretable latent factors, we consider the following partitions

$$\mathcal{H}(:, :, 1) = \mathcal{H}(:, :, 1) = \dots = \mathcal{H}(:, :, 5), \quad \text{PanCan12 dataset}$$

which enforces the similarity across third dimension, i.e., platform.

For the gene subgroups, we chose the Hallmark gene sets collection from MSigDB [47] and set $c_{i_n, j_n} = 1$ if genes belong to same subgroups. A gene smoothing function s_{i_n, j_n}^h is generated in the form of gene-gene interaction within each subgroup. We use the average of 10 multiple Gaussian kernels with various hyper-parameters, which give rise to better empirical results than other choices of kernels.

Test RMSE is used to measure the accuracy of tensor methods on this dataset. To obtain test RMSE, we split the PanCan12 tensor into training/testing data sets with a ratio of 9

Table 5.2: The test root mean square error (RMSE) of tensor methods on PanCan12 dataset.

Dataset	$[R_1, R_2, R_3]$	S-DCOT(R)	DCOT(R)	S-Tucker(R)	Tucker(R)
PanCan12	[20, 30, 5]	21.36e-2	22.19e-2	82.31e-2	84.73e-2
	[40, 60, 5]	12.01e-2	14.15e-2	38.18e-2	43.26e-2

(training) to 1 (testing). Table 5.3 indicates that the proposed DCOT has the best performance in terms of RMSE. The test RMSE of Tucker is $5\times$ higher than that of DCOT. Furthermore, test RMSE of S-DCOT is slightly higher or even better than that of Tucker and S-Tucker.

5.2.1. Recommender systems. Next, we employ S-DCOT for recommender systems and compare it with five competing factorization methods. Three methods are existing methods, namely, Bayesian probabilistic tensor factorization (BPTF) [89], the factorization machine (libFM)[63], and the Gaussian process factorization machine (GPFM) [58].⁶ In addition, we also investigate the performance of matrix factorization (MF) and a smooth variant of MF (S-MF) with the proposed linearized ADMM, which is the misspecified proposed method with $d = 2$ and ignoring contextual information.

We apply the proposed method to MovieLens 1M data collected by GroupLens Research⁷. This dataset contains 1,000,209 ratings of 3883 movies by 6040 users, and rating scores range from 1 to 5. Also, the MovieLens 1M dataset provides demographic information for the users (age, gender, occupation, zipcode), and genres and release dates of the movies.

We define day as a context for the DCOT recommender model detailed in Subsection 2.3.1. Having the length of the context determined, we need to create *time bands* in days. Time bands specify the time resolution of a day, which is also data dependent. We can create time bands with equal or different length. For this dataset, we used time bands of 1 hours. Events are assigned to time bands according to their time stamp. Thus, we can create the `[user, item, day, time bands]` tensor. We factorize this tensor using the DCOT model and we get feature vectors for each user, for each item, for each day, and for each time bands.

Since, we expect that at the same time offset in different days, the aggregated behavior of the users will be similar, we consider the following partitions

$$\mathcal{H}_{m_\kappa} = \mathcal{H}(:, :, m, \kappa), \quad \kappa = 1, \dots, R_4, \quad m = 1, \dots, R_3, \quad \text{Last.fm dataset,}$$

which enforces the similarity across members of R_4 .

For this application, in addition to heterogeneous core \mathcal{H} , we focus on utilizing user-item smoothing function to solve the cold-start issue. We classify users based on the quantiles of the number of their ratings and set $c_{i_n, j_n} = 1$ if users belong to same clusters. On the other hand, the items are classified based on their release dates and $c_{i_n, j_n} = 1$ if they belong to same clusters. We apply a Gaussian kernel with window size h as the median distance among all user-item pairs. For user-item pair, we compute s^h as in (2.4), and truncate them to keep only

⁶The codes can be obtained from <https://www.cs.cmu.edu/~lxiong/bptf/bptf.html>, <http://www.libfm.org/>, and <http://trungngv.github.io/gpfm/>, respectively.

⁷<http://grouplens.org/datasets/movielens>

Table 5.3: The root mean square error (RMSE) of completion methods on recommender systems dataset.

Dataset	Features	S-DCOT(R)	libFM	GPFM	BPTF	S-MF	MF
MovieLens 1M	20	0.962(0.003)	0.993(0.006)	1.020(0.004)	1.011(0.009)	0.971(0.004)	1.078 (0.005)
	40	0.941(0.006)	0.981(0.006)	0.979(0.004)	0.986(0.009)	0.957(0.004)	1.014 (0.005)

the five most similar users and items for each pair. We select the regularization parameter as $\lambda = \lambda_i = 10$, for $i = 1, 2, 3$.

Table 5.3 indicates that the proposed S-DCOT has the best performance in terms of RMSE. The RMSE of the proposed method is less than that of BPTF and libFM, illustrating that S-DCOT has better performance among the competing tensor factorization methods.

5.3. DCOT applied to subspace clustering and dictionary learning. Previous studies show that HOSVD is very powerful for clustering, especially in multiway data clustering tasks [53]. It can achieve similar or better performance than most of the state-of-the-art clustering algorithms for multiway data. Next, we evaluate the DCOT decomposition with OTV regularization on a clustering problem. We compare DCOT with HOSVD and also four classical dimensionality reduction methods, including Principle Component Analysis (PCA) [80], Linear Discriminant Analysis (LDA) [7], Locality Preserving Projections (LPP) [31], and Marginal Fisher Analysis (MFA) [92].

We evaluate our approach on the CMU and CASIA databases. The CASIA gait B database [93] comprises of indoor walking sequences from 124 subjects with 11 camera views and 10 clothing styles. We represent each walking sequence by the Gait Energy Image [54], which is resized into size 128×88 . All the images are vectorized, and the data set is arranged as a fourth-order tensor, three for the latent factors and one for the feature dimension. Thus, the size of data set is $(124 \times 11 \times 10 \times 11264)$. We use the average of 10 multiple Gaussian kernels. In our experiments, window size h is set at the average of all the pairwise distance.

To leverage the supervised information (i.e. subjects), we consider the following partitions

$$\begin{aligned}\mathcal{H}_{m_\kappa} &= \mathcal{H}(m, :, \kappa, :), \quad \kappa = 1, \dots, 21, \quad m = 1, \dots, 65, \quad \text{CMU database,} \\ \mathcal{H}_{m_\kappa} &= \mathcal{H}(:, m, \kappa, :), \quad \kappa = 1, \dots, 11, \quad m = 1, \dots, 10, \quad \text{CASIA database.}\end{aligned}$$

We randomly select ϖ subjects, where $\varpi = 10, 20, 30$, with 5 selected poses or illuminations in the CMU-PIE data set and with 4 selected views or clothing styles in the CASIA data set, respectively. The remaining samples in each database are used for testing. We employ a nearest neighbor classifier and repeat the procedure 5 times and average the results. To avoid the singularity of this problem, we use the first P principal coefficients determined by 95% energy for all the methods. Note that the MGE, LPP and MFA are manifold-based methods and need to determine the k nearest neighbors in their graphs. In all experiments, we set $k = 15$ for LPP, $k = 5$ or 30 for MFA with respect to the penalty graph, and $k = 24$ for MGE with respect to all of the three latent factors.

The overall performance is given in Table 5.4. We consider the following cases: “untrained pose (UP)”, “untrained illumination (UI)” that refers to a subset of testing data whose

Table 5.4: Average Detection Accuracy of Clustering (%) methods on the Face Databases .

Data		S-DCOT(H)	DCOT(H)	HOSVD	PCA	LPP	MFA	LDA
CMU	UP	35.13	36.38	29.10	36.16	32.81	34.24	33.19
	UI	96.24	98.41	90.39	75.39	83.90	92.14	89.15
CASIA	UP	68.19	67.14	66.29	55.34	58.18	50.29	62.17
	UI	88.31	86.11	83.19	80.33	84.34	82.29	83.21

corresponding factors (pose or illumination) are not available during training. DCOT achieves a high detection rate on the samples even when other complex factors are unobserved. DCOT significantly improves multilinear-based methods and better interprets the cross-factor variation hidden in multi-factor data, even when the factor variation is not given in the training stage. We believe the benefits mainly come from discriminative core structure of tensor, and similarity function which exploit all of the latent factors to embed factor-dependent data pairs in a unified way.

REFERENCES

- [1] G. ADOMAVICIUS AND A. TUZHILIN, *Toward the next generation of recommender systems: A survey of the state-of-the-art and possible extensions*, IEEE Transactions on Knowledge & Data Engineering, (2005), pp. 734–749.
- [2] G. ADOMAVICIUS AND A. TUZHILIN, *Context-aware recommender systems*, in Recommender systems handbook, Springer, 2011, pp. 217–253.
- [3] B. ALEXEEV, M. A. FORBES, AND J. TSIMERMAN, *Tensor rank: Some lower and upper bounds*, in Computational Complexity (CCC), 2011 IEEE 26th Annual Conference on, IEEE, 2011, pp. 283–291.
- [4] E. S. ALLMAN, P. D. JARVIS, J. A. RHODES, AND J. G. SUMNER, *Tensor rank, invariants, inequalities, and applications*, SIAM Journal on Matrix Analysis and Applications, 34 (2013), pp. 1014–1045.
- [5] M. T. BAHADORI, Q. R. YU, AND Y. LIU, *Fast multivariate spatio-temporal analysis via low rank tensor learning*, (2014), pp. 3491–3499.
- [6] M. BAHRI, Y. PANAGAKIS, AND S. P. ZAFEIRIOU, *Robust kronecker component analysis*, IEEE transactions on pattern analysis and machine intelligence, (2018).
- [7] P. N. BELHUMEUR, J. P. HESPANHA, AND D. J. KRIEGMAN, *Eigenfaces vs. fisherfaces: Recognition using class specific linear projection*, IEEE Transactions on pattern analysis and machine intelligence, 19 (1997), pp. 711–720.
- [8] X. S. A. Q. BEN DAI, JUNHUI WANG, *Smooth neighborhood recommender systems*, Journal of Machine Learning Research, 20 (2019), pp. 1–24.
- [9] X. BI, A. QU, X. SHEN, ET AL., *Multilayer tensor factorization with applications to recommender systems*, The Annals of Statistics, 46 (2018), pp. 3308–3333.
- [10] X. BI, A. QU, J. WANG, AND X. SHEN, *A group-specific recommender system*, Journal of the American Statistical Association, 112 (2017), pp. 1344–1353.
- [11] P. BILLINGSLEY, *Convergence of probability measures*, John Wiley & Sons, 2013.
- [12] J. BOGAERT, S. DYMARKOWSKI, A. M. TAYLOR, AND V. MUTHURANGU, *Clinical cardiac MRI*, Springer Science & Business Media, 2012.
- [13] J. BOLTE, S. SABACH, AND M. TEBoulLE, *Proximal alternating linearized minimization for nonconvex and nonsmooth problems*, Mathematical Programming, 146 (2014), pp. 459–494.
- [14] J. BOLTE, S. SABACH, AND M. TEBoulLE, *Proximal alternating linearized minimization or nonconvex and nonsmooth problems*, Mathematical Programming, 146 (2014), pp. 459–494.

- [15] R. H. BYRD, P. LU, J. NOCEDAL, AND C. ZHU, *A limited memory algorithm for bound constrained optimization*, SIAM Journal on Scientific Computing, 16 (1995), pp. 1190–1208.
- [16] E. J. CANDÈS, C. A. SING-LONG, AND J. D. TRZASKO, *Unbiased risk estimates for singular value thresholding and spectral estimators*, IEEE transactions on signal processing, 61 (2013), pp. 4643–4657.
- [17] J. D. CARROLL AND J.-J. CHANG, *Analysis of individual differences in multidimensional scaling via an n -way generalization of eckart-young decomposition*, Psychometrika, 35 (1970), pp. 283–319.
- [18] Y.-L. CHEN AND C.-T. HSU, *Multilinear graph embedding: Representation and regularization for images*, IEEE Transactions on Image Processing, 23 (2014), pp. 741–754.
- [19] Y.-L. CHEN, C.-T. HSU, AND H.-Y. M. LIAO, *Simultaneous tensor decomposition and completion using factor priors*, IEEE transactions on pattern analysis and machine intelligence, 36 (2013), pp. 577–591.
- [20] F. CHUNG AND L. LU, *Concentration inequalities and martingale inequalities: a survey*, Internet Mathematics, 3 (2006), pp. 79–127.
- [21] A. CICHOCKI, D. MANDIC, L. DE LATHAUWER, G. ZHOU, Q. ZHAO, C. CAIAFA, AND H. A. PHAN, *Tensor decompositions for signal processing applications: From two-way to multiway component analysis*, IEEE Signal Processing Magazine, 32 (2015), pp. 145–163.
- [22] L. DE LATHAUWER, B. DE MOOR, AND J. VANDEWALLE, *A multilinear singular value decomposition*, SIAM journal on Matrix Analysis and Applications, 21 (2000), pp. 1253–1278.
- [23] L. DE LATHAUWER, B. DE MOOR, AND J. VANDEWALLE, *On the best rank-1 and rank- (r_1, r_2, \dots, r_n) approximation of higher-order tensors*, SIAM journal on Matrix Analysis and Applications, 21 (2000), pp. 1324–1342.
- [24] V. DE SILVA AND L.-H. LIM, *Tensor rank and the ill-posedness of the best low-rank approximation problem*, SIAM Journal on Matrix Analysis and Applications, 30 (2008), pp. 1084–1127.
- [25] E. ELHAMIFAR, G. SAPIRO, AND S. S. SASTRY, *Dissimilarity-based sparse subset selection*, IEEE transactions on pattern analysis and machine intelligence, 38 (2015), pp. 2182–2197.
- [26] J. FAN, *Local polynomial modelling and its applications: monographs on statistics and applied probability 66*, Routledge, 2018.
- [27] E. FROLOV AND I. OSELEDETS, *Tensor methods and recommender systems*, Wiley Interdisciplinary Reviews: Data Mining and Knowledge Discovery, 7 (2017), p. e1201.
- [28] H. GE, J. CAVERLEE, AND H. LU, *Taper: A contextual tensor-based approach for personalized expert recommendation*, in Proceedings of the 10th ACM Conference on Recommender Systems, ACM, 2016, pp. 261–268.
- [29] J. HÅSTAD, *Tensor rank is np -complete*, Journal of Algorithms, 11 (1990), pp. 644–654.
- [30] S. HAWE, M. SEIBERT, AND M. KLEINSTEUBER, *Separable dictionary learning*, in Computer Vision and Pattern Recognition (CVPR), 2013 IEEE Conference on, IEEE, 2013, pp. 438–445.
- [31] X. HE, S. YAN, Y. HU, P. NIYOGI, AND H.-J. ZHANG, *Face recognition using laplacianfaces*, IEEE transactions on pattern analysis and machine intelligence, 27 (2005), pp. 328–340.
- [32] K. A. HOADLEY, C. YAU, D. M. WOLF, A. D. CHERNIACK, D. TAMBORERO, S. NG, M. D. LEISERSON, B. NIU, M. D. MCLELLAN, V. UZUNANGELOV, ET AL., *Multiplatform analysis of 12 cancer types reveals molecular classification within and across tissues of origin*, Cell, 158 (2014), pp. 929–944.
- [33] M. HOFREE, J. P. SHEN, H. CARTER, A. GROSS, AND T. IDEKER, *Network-based stratification of tumor mutations*, Nature methods, 10 (2013), p. 1108.
- [34] D. HONG, T. G. KOLDA, AND J. A. DUERSCH, *Generalized canonical polyadic tensor decomposition*, SIAM Review, (2019), <https://arxiv.org/abs/1808.07452>. in press.
- [35] M. HONG, Z.-Q. LUO, AND M. RAZAVIYAYN, *Convergence analysis of alternating direction method of multipliers for a family of nonconvex problems*, SIAM Journal on Optimization, 26 (2016), pp. 337–364.
- [36] V. HORE, A. VIÑUELA, A. BUIL, J. KNIGHT, M. I. MCCARTHY, K. SMALL, AND J. MARCHINI, *Tensor decomposition for multiple-tissue gene expression experiments*, Nature genetics, 48 (2016), p. 1094.
- [37] Z. JIANG, Z. LIN, AND L. S. DAVIS, *Label consistent k -svd: Learning a discriminative dictionary for recognition*, IEEE transactions on pattern analysis and machine intelligence, 35 (2013), pp. 2651–2664.
- [38] M. E. KILMER, K. BRAMAN, N. HAO, AND R. C. HOOVER, *Third-order tensors as operators on matrices: A theoretical and computational framework with applications in imaging*, SIAM Journal on Matrix Analysis and Applications, 34 (2013), pp. 148–172.
- [39] Y. KIM, R. EL-KAREH, J. SUN, H. YU, AND X. JIANG, *Discriminative and distinct phenotyping by constrained tensor factorization*, Scientific reports, 7 (2017), p. 1114.

- [40] T. G. KOLDA AND B. W. BADER, *Tensor decompositions and applications*, SIAM review, 51 (2009), pp. 455–500.
- [41] D. KRESSNER, M. STEINLECHNER, AND B. VANDEREYCKEN, *Low-rank tensor completion by riemannian optimization*, BIT Numerical Mathematics, 54 (2014), pp. 447–468.
- [42] N. KUMAR, A. C. BERG, P. N. BELHUMEUR, AND S. K. NAYAR, *Attribute and simile classifiers for face verification*, in 2009 IEEE 12th International Conference on Computer Vision, IEEE, pp. 365–372.
- [43] K. LANG, *Newsweeder: Learning to filter netnews*, in Machine Learning Proceedings 1995, Elsevier, 1995, pp. 331–339.
- [44] A. J. LAUB, *Matrix analysis for scientists and engineers*, vol. 91, Siam, 2005.
- [45] J. LEE, S. KIM, G. LEBANON, AND Y. SINGER, *Local low-rank matrix approximation*, in International Conference on Machine Learning, 2013, pp. 82–90.
- [46] J. LEE, S. OH, AND L. SAEL, *Gift: Guided and interpretable factorization for tensors with an application to large-scale multi-platform cancer analysis*, Bioinformatics, 34 (2018), pp. 4151–4158.
- [47] A. LIBERZON, C. BIRGER, H. THORVALDSDÓTTIR, M. GHANDI, J. P. MESIROV, AND P. TAMAYO, *The molecular signatures database hallmark gene set collection*, Cell systems, 1 (2015), pp. 417–425.
- [48] T. LIN, S. MA, AND S. ZHANG, *Iteration complexity analysis of multi-block admm for a family of convex minimization without strong convexity*, Journal of Scientific Computing, 69 (2016), pp. 52–81.
- [49] S. G. LINGALA, Y. HU, E. DiBELLA, AND M. JACOB, *Accelerated dynamic mri exploiting sparsity and low-rank structure: kt slr*, IEEE transactions on medical imaging, 30 (2011), pp. 1042–1054.
- [50] J. LIU, P. MUSIALSKI, P. WONKA, AND J. YE, *Tensor completion for estimating missing values in visual data*, IEEE transactions on pattern analysis and machine intelligence, 35 (2012), pp. 208–220.
- [51] J. LIU, P. MUSIALSKI, P. WONKA, AND J. YE, *Tensor completion for estimating missing values in visual data*, IEEE Transactions on Pattern Analysis and Machine Intelligence, 35 (2013), pp. 208–220.
- [52] E. F. LOCK AND G. LI, *Supervised multiway factorization*, Electronic journal of statistics, 12 (2018), p. 1150.
- [53] H. LU, K. N. PLATANOTIS, AND A. N. VENETSANOPOULOS, *A survey of multilinear subspace learning for tensor data*, Pattern Recognition, 44 (2011), pp. 1540–1551.
- [54] J. MAN AND B. BHANU, *Individual recognition using gait energy image*, IEEE transactions on pattern analysis and machine intelligence, 28 (2006), pp. 316–322.
- [55] J.-J. MOREAU, *Proximité et dualité dans un espace hilbertien*, Bulletin de la Société mathématique de France, 93 (1965), pp. 273–299.
- [56] A. NARITA, K. HAYASHI, R. TOMIOKA, AND H. KASHIMA, *Tensor factorization using auxiliary information*, Data Mining and Knowledge Discovery, 25 (2012), pp. 298–324.
- [57] C. G. A. NETWORK ET AL., *Comprehensive molecular portraits of human breast tumours*, Nature, 490 (2012), p. 61.
- [58] T. V. NGUYEN, A. KARATZOGLOU, AND L. BALTRUNAS, *Gaussian process factorization machines for context-aware recommendations*, in Proceedings of the 37th international ACM SIGIR conference on Research & development in information retrieval, ACM, 2014, pp. 63–72.
- [59] L. OMBERG, K. ELLROTT, Y. YUAN, C. KANDOTH, C. WONG, M. R. KELLEN, S. H. FRIEND, J. STUART, H. LIANG, AND A. A. MARGOLIN, *Enabling transparent and collaborative computational analysis of 12 tumor types within the cancer genome atlas*, Nature genetics, 45 (2013), p. 1121.
- [60] I. V. OSELEDETS, *Tensor-train decomposition*, SIAM Journal on Scientific Computing, 33 (2011), pp. 2295–2317.
- [61] N. PARIKH, S. BOYD, ET AL., *Proximal algorithms*, Foundations and Trends® in Optimization, 1 (2014), pp. 127–239.
- [62] N. QI, Y. SHI, X. SUN, J. WANG, B. YIN, AND J. GAO, *Multi-dimensional sparse models*, IEEE transactions on pattern analysis and machine intelligence, 40 (2018), pp. 163–178.
- [63] S. RENDLE, *Factorization machines with libfm*, ACM Transactions on Intelligent Systems and Technology (TIST), 3 (2012), p. 57.
- [64] R. T. ROCKAFELLAR AND R. J.-B. WETS, *Variational analysis*, vol. 317, Springer Science & Business Media, 2009.
- [65] J. L. R. V. J. P. X. L. S. SMITH, J. W. CHOI AND G. KARYPIS, *Frostt: The formidable repository of open sparse tensors and tools*, 2017, <http://frostt.io/>.
- [66] D. W. SCOTT, *Multivariate density estimation and visualization*, in Handbook of computational statistics,

- Springer, 2012, pp. 549–569.
- [67] Z. SHAKERI, W. U. BAJWA, AND A. D. SARWATE, *Minimax lower bounds on dictionary learning for tensor data*, IEEE Transactions on Information Theory, (2018).
 - [68] X. SHEN, *On the method of penalization*, Statistica Sinica, (1998), pp. 337–357.
 - [69] N. D. SIDIROPOULOS, L. DE LATHAUWER, X. FU, K. HUANG, E. E. PAPALEXAKIS, AND C. FALOUTSOS, *Tensor decomposition for signal processing and machine learning*, IEEE Transactions on Signal Processing, 65 (2017), pp. 3551–3582.
 - [70] T. SIM, S. BAKER, AND M. BSAT, *The cmu pose, illumination, and expression (pie) database*, in Automatic Face and Gesture Recognition, 2002. Proceedings. Fifth IEEE International Conference on, IEEE, 2002, pp. 53–58.
 - [71] N. SIMON, J. FRIEDMAN, T. HASTIE, AND R. TIBSHIRANI, *A sparse-group lasso*, Journal of Computational and Graphical Statistics, 22 (2013), pp. 231–245.
 - [72] Q. SONG, H. GE, J. CAVERLEE, AND X. HU, *Tensor completion algorithms in big data analytics*, arXiv preprint arXiv:1711.10105, (2017).
 - [73] Y.-H. TAGUCHI, *Identification of candidate drugs using tensor-decomposition-based unsupervised feature extraction in integrated analysis of gene expression between diseases and drugmatrix datasets*, Scientific reports, 7 (2017), p. 13733.
 - [74] D. A. TARZANAGH AND G. MICHAILIDIS, *Estimation of graphical models through structured norm minimization*, Journal of Machine Learning Research, 18 (2018), pp. 1–48.
 - [75] D. A. TARZANAGH AND G. MICHAILIDIS, *Fast randomized algorithms for t-product based tensor operations and decompositions with applications to imaging data*, SIAM Journal on Imaging Sciences, 11 (2018), pp. 2629–2664.
 - [76] D. A. TARZANAGH AND M. R. PEYGHAMI, *A new regularized limited memory bfgs-type method based on modified secant conditions for unconstrained optimization problems*, Journal of Global Optimization, 63 (2015), pp. 709–728.
 - [77] R. TIBSHIRANI AND T. HASTIE, *Local likelihood estimation*, Journal of the American Statistical Association, 82 (1987), pp. 559–567.
 - [78] L. R. TUCKER, *The extension of factor analysis to three-dimensional matrices*, in Contributions to mathematical psychology., H. Gulliksen and N. Frederiksen, eds., Holt, Rinehart and Winston, New York, 1964, pp. 110–127.
 - [79] L. R. TUCKER, *Some mathematical notes on three-mode factor analysis*, Psychometrika, 31 (1966), pp. 279–311.
 - [80] M. A. TURK AND A. P. PENTLAND, *Face recognition using eigenfaces*, in Computer Vision and Pattern Recognition, 1991. Proceedings CVPR’91., IEEE Computer Society Conference on, IEEE, 1991, pp. 586–591.
 - [81] K. VERBERT, N. MANOUSELIS, X. OCHOA, M. WOLPERS, H. DRACHSLER, I. BOSNIC, AND E. DUVAL, *Context-aware recommender systems for learning: a survey and future challenges*, IEEE Transactions on Learning Technologies, 5 (2012), pp. 318–335.
 - [82] P. VIEU, *Nonparametric regression: optimal local bandwidth choice*, Journal of the Royal Statistical Society: Series B (Methodological), 53 (1991), pp. 453–464.
 - [83] M. P. WAND AND M. C. JONES, *Kernel smoothing*, Chapman and Hall/CRC, 1994.
 - [84] Y. WANG, R. CHEN, J. GHOSH, J. C. DENNY, A. KHO, Y. CHEN, B. A. MALIN, AND J. SUN, *Rubik: Knowledge guided tensor factorization and completion for health data analytics*, in Proceedings of the 21th ACM SIGKDD International Conference on Knowledge Discovery and Data Mining, ACM, 2015, pp. 1265–1274.
 - [85] L. WASSERMAN, *All of nonparametric statistics*, Springer Science & Business Media, 2006.
 - [86] J. N. WEINSTEIN, E. A. COLLISON, G. B. MILLS, K. R. M. SHAW, B. A. OZENBERGER, K. ELLROTT, I. SHMULEVICH, C. SANDER, J. M. STUART, C. G. A. R. NETWORK, ET AL., *The cancer genome atlas pan-cancer analysis project*, Nature genetics, 45 (2013), p. 1113.
 - [87] Z. WEN AND W. YIN, *A feasible method for optimization with orthogonality constraints*, Mathematical Programming, 142 (2013), pp. 397–434.
 - [88] W. H. WONG, X. SHEN, ET AL., *Probability inequalities for likelihood ratios and convergence rates of sieve mles*, The Annals of Statistics, 23 (1995), pp. 339–362.
 - [89] L. XIONG, X. CHEN, T.-K. HUANG, J. SCHNEIDER, AND J. G. CARBONELL, *Temporal collaborative*

- filtering with bayesian probabilistic tensor factorization*, in Proceedings of the 2010 SIAM international conference on data mining, SIAM, 2010, pp. 211–222.
- [90] Y. XU, R. HAO, W. YIN, AND Z. SU, *Parallel matrix factorization for low-rank tensor completion*, arXiv preprint arXiv:1312.1254, (2013).
- [91] Y. XU AND W. YIN, *A block coordinate descent method for regularized multiconvex optimization with applications to nonnegative tensor factorization and completion*, SIAM Journal on imaging sciences, 6 (2013), pp. 1758–1789.
- [92] S. YAN, D. XU, B. ZHANG, H.-J. ZHANG, Q. YANG, AND S. LIN, *Graph embedding and extensions: A general framework for dimensionality reduction*, IEEE transactions on pattern analysis and machine intelligence, 29 (2007), pp. 40–51.
- [93] S. YU, D. TAN, AND T. TAN, *A framework for evaluating the effect of view angle, clothing and carrying condition on gait recognition*, in Pattern Recognition, 2006. ICPR 2006. 18th International Conference on, vol. 4, IEEE, pp. 441–444.
- [94] Z. ZHANG AND S. AERON, *Exact tensor completion using t-svd*, IEEE Transactions on Signal Processing, (2016).
- [95] Z. ZHANG, G. ELY, S. AERON, N. HAO, AND M. KILMER, *Novel methods for multilinear data completion and de-noising based on tensor-svd*, in Proceedings of the IEEE Conference on Computer Vision and Pattern Recognition, 2014, pp. 3842–3849.
- [96] Q. ZHAO, L. ZHANG, AND A. CICHOCKI, *Bayesian cp factorization of incomplete tensors with automatic rank determination*, IEEE transactions on pattern analysis and machine intelligence, 37 (2015), pp. 1751–1763.

Appendix A: Useful properties of the Kronecker product. As the properties of Kronecker product are not always widely known, we have compiled a list of some fundamental algebraic relations we use [44].

1. Sum or difference of Kronecker product:

$$\begin{aligned} c_A(A_1 \otimes \cdots \otimes A_K) + c_B(B_1 \otimes \cdots \otimes B_K) \\ = (c_A A_1 + c_B B_1) \otimes \cdots \otimes (c_A A_K + c_B B_K). \end{aligned}$$

2. Product of Kronecker product :

$$\begin{aligned} c(A_1 \otimes \cdots \otimes A_K)(B_1 \otimes \cdots \otimes B_K) \\ = (cA_1 B_1) \otimes \cdots \otimes (cB_A K B_K). \end{aligned}$$

3. Eigendecomposition: If $A_k = U_k \Lambda_k U_k^T$ are the eigendecompositions of the factors, then

$$A_1 \otimes \cdots \otimes A_K = (U_1 \otimes \cdots \otimes U_K)(\Lambda_1 \otimes \cdots \otimes \Lambda_K)(U_1 \otimes \cdots \otimes U_K)^T$$

is the eigendecomposition of $A_1 \otimes \cdots \otimes A_K$.

4. Schatten- p norm:

$$\|A_1 \otimes \cdots \otimes A_K\|_p = \prod_{k=1}^K \|A_k\|_p.$$

Appendix B: Updating parameters in Algorithm 3.1. This section provides detailed implementation of the linearized ADMM method for solving problem (2.3). As we discussed in the introduction, the proposed algorithm can be viewed as a ADMM version of the recent PALM algorithm [13]. Before presenting the algorithm it will be convenient to recall the

Table 5.5: Basic notation and product

$\mathcal{A}, \mathbf{A}, \mathbf{a}, a$	tensor, matrix, vector, scalar
$\mathbf{A} = [\mathbf{a}_1, \mathbf{a}_2, \dots, \mathbf{a}_R]$	matrix \mathbf{A} with column vectors \mathbf{a}_r
$a_{i_1 \dots i_N}$	entry of tensor $\mathcal{A} \in \mathbb{R}^{I_1 \times \dots \times I_N}$
$\mathbf{a}(:, i_2, \dots, i_N)$	fiber of tensor \mathcal{A} obtained by fixing all but one index
$\mathbf{A}(:, :, i_3, \dots, i_N)$	matrix slice of tensor \mathcal{A} obtained by fixing all but two indices
$\mathcal{A}(\mathcal{I}_1, \mathcal{I}_2, \dots, \mathcal{I}_N)$	subtensor of \mathcal{A} obtained by restricting indices to belong to subsets $\mathcal{I}_n \subseteq [I_n] \equiv \{1, 2, \dots, I_n\}$
$\mathbf{A}_{(n)} \in \mathbb{R}^{I_n \times I_1 I_2 \dots I_{n-1} I_{n+1} \dots I_N}$	mode- n matricization of tensor $\mathcal{A} \in \mathbb{R}^{I_1 \times I_2 \times \dots \times I_N}$ whose entry at row i_n and column $(i_1 - 1)I_2 \dots I_{n-1} I_{n+1} \dots I_N + \dots + (i_{N-1} - 1)I_N + i_N$ is equal to $a_{i_1 \dots i_N}$
$\text{vec}(\mathcal{A}) \in \mathbb{R}^{I_N I_{N-1} \dots I_1}$	vectorization of tensor $\mathcal{A} \in \mathbb{R}^{I_1 \times I_2 \times \dots \times I_N}$ with the entry at position $i_1 + \sum_{k=2}^N [(i_k - 1)I_1 I_2 \dots I_{k-1}]$ equal to $a_{i_1 \dots i_N}$
$\langle \mathcal{X}, \mathcal{Y} \rangle := \text{vec}(\mathcal{X})^T \text{vec}(\mathcal{Y})$	inner product of two tensors $\mathcal{X}, \mathcal{Y} \in \mathbb{R}^{I_1 \times I_2 \times \dots \times I_N}$
$\mathbf{D} = \text{diag}(a_1, a_2, \dots, a_R)$	diagonal matrix with $d_{rr} = a_r$
$\mathbf{A}^\top, \mathbf{A}^{-1}, \mathbf{A}^\dagger$	transpose, inverse, and Moore-Penrose pseudo-inverse
$\ \mathbf{X}\ _F, \ \mathbf{X}\ _*, \ \mathbf{X}\ _1$	Frobenius norm, the nuclear norm or trace norm as the sum of singular values of \mathbf{X} , and the ℓ_1 norm.
$\ \mathbf{X}\ _2, \ \mathbf{X}\ _{b,a}$	The spectral norm as the largest singular value of matrix, the ℓ_a/ℓ_b norm as the ℓ_a norm of the vector formed by the ℓ_b norm of every row.
$\mathcal{C} = \mathcal{A} \times_n \mathbf{U}$	mode- n product of $\mathcal{A} \in \mathbb{R}^{I_1 \times I_2 \times \dots \times I_N}$ and $\mathbf{U} \in \mathbb{R}^{j_N \times I_n}$ yields $\mathcal{C} \in \mathbb{R}^{I_1 \times \dots \times I_{n-1} \times j_N \times I_{n+1} \times \dots \times I_N}$ with entries $c_{i_1 \dots i_{n-1} j_N i_{n+1} \dots i_N} = \sum_{i_n=1}^{I_n} a_{i_1 \dots i_{n-1} i_n i_{n+1} \dots i_N} b_{j_N i_n}$ and matrix representation $\mathbf{C}_{(n)} = \mathbf{U} \mathbf{A}_{(n)}$
$\mathcal{C} = [\mathcal{A}; \mathbf{U}^{(1)}, \mathbf{U}^{(2)}, \dots, \mathbf{U}^{(N)}]$	full multilinear product, $\mathcal{C} = \mathcal{A} \times_1 \mathbf{U}^{(1)} \times_2 \mathbf{U}^{(2)} \dots \times_N \mathbf{U}^{(N)}$
$\mathcal{C} = \mathcal{A} \circ \mathcal{B}$	tensor or outer product of $\mathcal{A} \in \mathbb{R}^{I_1 \times I_2 \times \dots \times I_N}$ and $\mathcal{B} \in \mathbb{R}^{J_1 \times J_2 \times \dots \times J_N}$ yields $\mathcal{C} \in \mathbb{R}^{I_1 \times I_2 \times \dots \times I_N \times J_1 \times J_2 \times \dots \times J_N}$ with entries $c_{i_1 \dots i_N j_1 \dots j_N} = a_{i_1 \dots i_N} b_{j_1 \dots j_N}$
$\mathcal{X} = \mathbf{a}^{(1)} \circ \mathbf{a}^{(2)} \circ \dots \circ \mathbf{a}^{(N)}$	tensor or outer product of vectors $\mathbf{a}^{(n)} \in \mathbb{R}^{I_n}$ ($n = 1, \dots, N$) yields a rank-1 tensor $\mathcal{X} \in \mathbb{R}^{I_1 \times I_2 \times \dots \times I_N}$ with entries
$\mathbf{C} = \mathbf{A} \otimes \mathbf{U}$	Kronecker product of $\mathbf{A} \in \mathbb{R}^{I_1 \times I_2}$ and $\mathbf{U} \in \mathbb{R}^{J_1 \times J_2}$ yields $\mathbf{C} \in \mathbb{R}^{I_1 J_1 \times I_2 J_2}$ with entries $c_{(i_1-1)J_1+j_1, (i_2-1)J_2+j_2} = a_{i_1 i_2} b_{j_1 j_2}$
$\mathbf{C} = \mathbf{A} \oplus \mathbf{U}$	Kronecker sum of $\mathbf{A} \in \mathbb{R}^{I_1 \times I_2}$ and $\mathbf{U} \in \mathbb{R}^{J_1 \times J_2}$ yields $\mathbf{C} \in \mathbb{R}^{I_1 J_1 \times I_2 J_2}$ with entries
$\mathbf{C} = \mathbf{A} \odot \mathbf{U}$	Khatri-Rao product of $\mathbf{A} = [\mathbf{a}_1, \dots, \mathbf{a}_R] \in \mathbb{R}^{I \times R}$ and $\mathbf{U} = [\mathbf{u}_1, \dots, \mathbf{u}_R] \in \mathbb{R}^{J \times R}$ yields $\mathbf{C} \in \mathbb{R}^{IJ \times R}$ with columns $\mathbf{c}_r = \mathbf{a}_r \otimes \mathbf{b}_r$

definition of the Moreau proximal mapping [55]. Given a proper and lower semicontinuous function $J : \mathbb{R}^d \rightarrow (-\infty, \infty]$, the proximal mapping associated with J is defined by

$$(\cdot 2) \quad \text{prox}_\rho^J(p) := \operatorname{argmin} \left\{ J(q) + \frac{\rho}{2} \|q - p\|^2 : q \in \mathbb{R}^d \right\}, \quad (\rho > 0).$$

The following result can be found in [64].

Proposition .1. [13] *Let Assumption 2.2 holds. Then, for every $t \in (0, \infty)$ the set $\text{prox}_t^J(u)$ is nonempty and compact.*

To keep things simple, we also define

$$\begin{aligned} \mathcal{R}_k^{\mathcal{H}} &= \mathbf{z}_k - \gamma^{-1} \mathbf{y}_k - [\mathcal{H}_k; \mathbf{U}_{k+1}^{(1)}, \dots, \mathbf{U}_{k+1}^{(N)}], \\ \mathcal{R}_k^{\mathcal{G}} &= \mathbf{z}_k - \gamma^{-1} \mathbf{y}_k - [\mathcal{G}_{k+1}; \mathbf{U}_{k+1}^{(1)}, \dots, \mathbf{U}_{k+1}^{(N)}], \\ \mathcal{R}_k^{\mathcal{Y}} &= \gamma^{-1} \mathbf{y}_k - [\mathcal{G}_{k+1} + \mathcal{H}_{k+1}; \mathbf{U}_{k+1}^{(1)}, \dots, \mathbf{U}_{k+1}^{(N)}]. \end{aligned}$$

.0.1. Updating $\mathbf{U}^{(n)}$. We need the gradient of the function $\bar{\mathcal{L}}(\mathcal{T})$ in (3.11) with respect to the factor matrices. Let

$$(\cdot 3) \quad \mathbf{Z}_{(n)}^t = (\mathcal{G}_{(n)} + \mathcal{H}_{(n)}) \left(\bigotimes_{t \neq n} \mathbf{U}^{(t)} \right)^\top.$$

Now, using (3.3) and (3), we obtain

$$(\cdot 4) \quad \nabla_{\mathbf{U}^{(n)}} \bar{\mathcal{L}}(\mathcal{T}^{\mathbf{U}^{(n)}}) = \gamma (\mathbf{U}^{(n)} \mathbf{Z}_{(n)}^t - \mathbf{z}_{(n)} + \gamma^{-1} \mathbf{y}_{(n)}) \mathbf{Z}_{(n)}^{t\top}.$$

Substituting (4) into (3.12), we obtain

$$\begin{aligned} \mathbf{U}_{k+1}^{(n)} &= \operatorname{argmin}_{\mathbf{U}^{(n)}} \lambda_{3,n} J_{3,n}(\mathbf{U}^{(n)}) + \langle \nabla_{\mathbf{U}^{(n)}} \bar{\mathcal{L}}(\mathcal{T}_k^{\mathbf{U}^{(n)}}), \mathbf{U}^{(n)} - \mathbf{U}_k^{(n)} \rangle \\ (\cdot 5) \quad &+ \frac{\varrho^n}{2} \|\mathbf{U}^{(n)} - \mathbf{U}_k^{(n)}\|_F^2, \end{aligned}$$

where ϱ^n is a constant equal or greater than the Lipschitz of the gradient $\nabla \bar{\mathcal{L}}(\mathcal{T}^{\mathbf{U}^{(n)}})$.

It follows from (2) that (5) has the following solution

$$(\cdot 6) \quad \mathbf{U}_{k+1}^{(n)} = \text{prox}_{\varrho^n}^{J_{3,n}} \left(\mathbf{U}_k^{(n)} - \frac{1}{\varrho^n} \nabla \bar{\mathcal{L}}(\mathcal{T}_k^{\mathbf{U}_k^{(n)}}), \frac{\lambda_{3,n}}{\varrho^n} \right).$$

It is worth mentioning that we can use (6) for different choices of penalty functions. As discussed in (2.3), typical examples of the function $J_{3,n}(\mathbf{U}^{(n)})$ include $\|\mathbf{U}^{(n)}\|_1$, $\|\mathbf{U}^{(n)}\|_*$ or the indicator of a closed convex set. For example if $J_{3,n}(\mathbf{U}^{(n)}) = \|\mathbf{U}^{(n)}\|_1$, we can apply the ℓ_1 proxiaml operator [61]. We also note that the Lipschitz constant of $\nabla \bar{\mathcal{L}}(\mathcal{T}^{\mathbf{U}^{(n)}})$ is defined by $\sigma_1(\gamma \mathbf{Z}_{(n)}^t \mathbf{Z}_{(n)}^{t\top})$, where σ_1 denotes the largest singular value of a matrix.

.0.2. Updating \mathcal{G} . To minimize the sub-lagrange function with respect to \mathcal{G} , using (3.13), we have

$$\mathcal{G}_{k+1} = \operatorname{argmin}_{\mathcal{G}} \langle \nabla \bar{\mathcal{L}}(\mathcal{T}_k^{\mathcal{G}}), \mathcal{G} - \mathcal{G}_k \rangle + \lambda_1 J_1(\mathcal{G}) + \frac{\varrho^g}{2} \|\mathcal{G} - \mathcal{G}_k\|_F^2$$

From (3.11) and (.3), the gradient $\nabla \bar{\mathcal{L}}(\mathcal{T}_k^{\mathcal{H}})$ is equal to

$$\nabla_{\mathcal{G}} \left(\frac{\gamma}{2} \|\mathcal{G} \times_1 \mathbf{U}_{k+1}^{(1)} \cdots \times_N \mathbf{U}_{k+1}^{(N)} - \mathcal{R}_k^{\mathcal{H}}\|_F \right).$$

Let $\mathbf{r}_k^h = \operatorname{vec}(\mathcal{R}_k^{\mathcal{H}})$ and $\mathbf{g} = \operatorname{vec}(\mathcal{G})$. Then, we have

$$\|\mathbf{U}_{k+1} \mathbf{g} - \mathbf{r}_k^h\|_F^2 = \sum_{r_1 \cdots r_N} \sum_{i_1 \cdots i_N} ((\mathbf{U}_{k+1})_{i_1 \cdots i_N, r_1 \cdots r_N} \mathbf{g}_{r_1 \cdots r_N} - (\mathbf{r}_k^h)_{i_1 \cdots i_N})^2,$$

where $\mathbf{U}_{i_1 \cdots i_N, r_1 \cdots r_N} = \mathbf{U}(i_1 \cdots i_N, r_1 \cdots r_N)$. Using the above formulation, we have

$$(.7) \quad (\nabla \bar{\mathcal{L}}(\mathcal{T}_k^{\mathcal{G}}))_{r_1 \cdots r_N} = \gamma \sum_{i_1 \cdots i_N} (\mathbf{U}_{k+1})_{i_1 \cdots i_N, r_1 \cdots r_N} ((\mathbf{U}_{k+1})_{i_1 \cdots i_N, r_1 \cdots r_N} \mathbf{g}_{r_1 \cdots r_N} - (\mathbf{r}_k^h)_{i_1 \cdots i_N}).$$

Using (3.13) and (.7), we have

$$(.8) \quad \mathcal{G}_{k+1} = \operatorname{prox}_{\varrho^g}^{J_1} \left(\mathcal{G}_k - \frac{1}{\varrho^g} \nabla \bar{\mathcal{L}}(\mathcal{T}_k^{\mathcal{G}}), \frac{\lambda_1}{\varrho^g} \right).$$

.0.3. Updating \mathcal{H} . To minimize the sub-Lagrangian function w.r.t. \mathcal{H} , using (3.14), we have

$$\mathcal{H}_{k+1} = \operatorname{argmin}_{\mathcal{H}} \langle \nabla \bar{\mathcal{L}}(\mathcal{T}_k^{\mathcal{H}_k}), \mathcal{H} - \mathcal{H}_k \rangle + \lambda_2 J_2(\mathcal{H}) + \frac{\varrho^h}{2} \|\mathcal{H} - \mathcal{H}_k\|_F^2.$$

Since the above problem is separable w.r.t $\{\mathcal{H}_{m_\pi}\}_{m=1}^M$, for each subject $m \in [M]$, we have

$$(.9) \quad \mathcal{H}_{m_1} = \mathcal{H}_{m_2} = \cdots = \mathcal{H}_{m_\pi},$$

where

$$\mathcal{H}_{m,k+1} = \operatorname{argmin}_{\mathcal{H}_{m_\pi}} \langle \nabla \bar{\mathcal{L}}(\mathcal{T}_k^{\mathcal{H}_{m_\pi}}), \mathcal{H}_{m_\pi} - \mathcal{H}_{m_\pi,k} \rangle + \lambda_2 J_2(\mathcal{H}_{m_\pi}) + \frac{\varrho^h}{2} \|\mathcal{H}_{m_\pi} - \mathcal{H}_{m_\pi,k}\|_F^2.$$

We note that the gradient $\nabla \bar{\mathcal{L}}(\mathcal{T}_k^{\mathcal{H}_{m_\pi}})$ is equal to

$$\nabla_{\mathcal{H}_{m_\pi}} \left(\frac{\gamma}{2} \|\mathcal{H} \times_1 \mathbf{U}_{k+1}^{(1)} \cdots \times_N \mathbf{U}_{k+1}^{(N)} - \mathcal{R}_k^{\mathcal{G}}\|_F \right).$$

Let $\mathbf{r}_k^g = \operatorname{vec}(\mathcal{R}_k^{\mathcal{G}})$ and $\mathbf{h} = \operatorname{vec}(\mathcal{H})$. Then, we obtain

$$(.10) \quad \|\mathbf{U}_{k+1} \mathbf{h} - \mathbf{r}_k^g\|_F^2 = \sum_{r_1 \cdots r_N} \sum_{i_1 \cdots i_N} ((\mathbf{U}_{k+1})_{i_1 i_2 \cdots i_N, r_1 \cdots r_N} \mathbf{h}_{r_1 \cdots r_N} - (\mathbf{r}_k^g)_{i_1 \cdots i_N})^2.$$

Hence

$$(11) \quad (\nabla \bar{\mathcal{L}}(\mathcal{T}^{\mathcal{H}_{m\pi}}))_{r_1 \dots r_N} = \gamma \sum_{r_1 \dots r_N \in \mathcal{H}_m} \sum_{i_1 \dots i_N} (\mathbf{U}_{k+1})_{i_1 \dots i_N, r_1 \dots r_N} ((\mathbf{U}_{k+1})_{i_1 \dots i_N, r_1 \dots r_N} \mathbf{h}_{r_1 \dots r_N} - (\mathbf{r}_k^g)_{i_1 \dots i_N}).$$

Using (11) and (3.14), we have

$$(12) \quad \mathcal{H}_{m\pi, k+1} = \text{Prox}_{\varrho^h}^{J_2} \left(\mathcal{H}_{m\pi, k} - \frac{1}{\varrho^h} \nabla \bar{\mathcal{L}}(\mathcal{T}_k^{\mathcal{H}_{m\pi, k}}), \frac{\lambda_2}{\varrho^h} \right), \quad m = 1, 2, \dots, M.$$

Finally, we set

$$(13) \quad \mathcal{H}_{m_1, k+1} = \mathcal{H}_{m_2, k+1} = \dots = \mathcal{H}_{m_\pi, k+1}.$$

.0.4. Updating incomplete tensor \mathcal{Z} . We derive an explicit formulation of the element-wise gradient w.r.t. \mathcal{Z} along with a straightforward way of handling missing data. To do so, from (3.9), we have

$$(14) \quad \mathcal{Z}_{k+1} = \underset{\mathcal{Z}}{\text{argmin}} \left\{ \mathcal{L}(\mathcal{T}_k^{\mathcal{Z}}) = F(s^h, \mathcal{X}; \mathcal{Z}) + \frac{\gamma}{2} \|\mathcal{Z} - \mathcal{R}_k^y\|_F^2 \right\}.$$

Following [34], we provide a generalized framework for computing gradients and handling missing data that enables the use of standard optimization methods for solving (14). Note that the gradient of objective in (14) w.r.t $z_{i_1 \dots i_N} \in \Omega$ is defined as follows

$$(15) \quad (\nabla \bar{\mathcal{L}}(\mathcal{T}_k^{\mathcal{Z}}))_{i_1 \dots i_N} = \nabla_{z_{i_1 \dots i_N}} (f(s^h, z_{i_1 \dots i_N}, x_{i_1 \dots i_N})) + \gamma \sum_{i_1 \dots i_N} (z_{i_1 \dots i_N} - (r_k^z)_{i_1 \dots i_N}),$$

where $f(., ., .)$ and $\mathcal{R}^{\mathcal{Z}}$ are defined in (2.7) and (3), respectively. Hence, (3.9) can be solved via a gradient-based optimization method.

Appendix C: Convergence analysis of linearized ADMM. In order to prove the global convergence result of our algorithm for DCOT, we need to introduce adequate and necessary material on the nonsmooth Kurdyka-Lojasiewicz property (for more details see [13]).

The next result shows that Algorithm 3.1 provides sufficient decrease of the augmented Lagrangian \mathcal{L} in each iteration.

Lemma 2. *Let Assumption 2.2 hold and $\gamma > L$, $\varrho^g > L^g$, $\varrho^h > L^h$, and $\varrho^n > L^n$ for $n = 1, 2, \dots, N$, where L^n, L^g, L^h and L are Lipschitz constants of the gradients of Lagrangian function \mathcal{L} w.r.t $\{\mathbf{U}^{(n)}\}_{n=1}^N, \mathcal{G}, \mathcal{H}$ and \mathcal{Z} , respectively. Then, for the sequence $\{\mathcal{T}_k\}_{k \geq 0}$ generated by Algorithm 3.1, we have*

$$(16) \quad \begin{aligned} \mathcal{L}(\mathcal{T}_k^{\mathbf{U}_k^{(n)}}) - \mathcal{L}(\mathcal{T}_{k+1}^{\mathbf{U}_{k+1}^{(n)}}) - \frac{\varrho^{(n)} - L^{(n)}}{2} \|\mathbf{U}_k^{(n)} - \mathbf{U}_{k+1}^{(n)}\|_F^2 &\geq 0, \quad n = 1, \dots, N, \\ \mathcal{L}(\mathcal{T}_k^{\mathcal{G}_k}) - \mathcal{L}(\mathcal{T}_{k+1}^{\mathcal{G}_{k+1}}) - \frac{\varrho^g - L^g}{2} \|\mathcal{G}_k - \mathcal{G}_{k+1}\|_F^2 &\geq 0, \\ \mathcal{L}(\mathcal{T}_k^{\mathcal{H}_k}) - \mathcal{L}(\mathcal{T}_{k+1}^{\mathcal{H}_{k+1}}) - \frac{\varrho^h - L^h}{2} \|\mathcal{H}_k - \mathcal{H}_{k+1}\|_F^2 &\geq 0, \\ \mathcal{L}(\mathcal{T}_k^{\mathcal{Z}_k}) - \mathcal{L}(\mathcal{T}_{k+1}^{\mathcal{Z}_{k+1}}) - \frac{\gamma - L}{2} \|\mathcal{Z}_k - \mathcal{Z}_{k+1}\|_F^2 &\geq 0. \end{aligned}$$

Proof. We note that the function $\mathcal{L}(\mathcal{T}_k^{\mathbf{z}})$ in (.14) is strongly convex w.r.t. \mathbf{z} whenever $\gamma > L$, where L is a Lipschitz constant for $\nabla F(s^h, \mathbf{x}; \mathbf{z})$; see, [Assumption 2.2](#). Thus, we have

$$\begin{aligned} \mathcal{L}(\mathcal{T}_{k+1}^{\mathbf{z}_{k+1}}) - \mathcal{L}(\mathcal{T}_k^{\mathbf{z}_k}) &= F(s^h, \mathbf{x}; \mathbf{z}_{k+1}) - F(s^h, \mathbf{x}; \mathbf{z}_k) \\ &\quad + \frac{\gamma}{2} \|(\mathcal{G}_{k+1} + \mathcal{H}_{k+1}) \times_1 \mathbf{U}_{k+1}^{(1)} \cdots \times_N \mathbf{U}_{k+1}^{(N)} - \mathbf{z}_{k+1} - \frac{1}{\gamma} \mathbf{y}_{k+1}\|_F^2 \\ &\quad - \frac{\gamma}{2} \|(\mathcal{G}_k + \mathcal{H}_k) \times_1 \mathbf{U}_k^{(1)} \cdots \times_N \mathbf{U}_k^{(N)} - \mathbf{z}_k - \frac{1}{\gamma} \mathbf{y}_k\|_F^2 \\ &\leq \langle \nabla \mathcal{L}(\mathcal{T}_k^{\mathbf{z}_{k+1}}), \mathbf{z}_{k+1} - \mathbf{z}_k \rangle - \frac{\gamma - L}{2} \|\mathbf{z}_{k+1} - \mathbf{z}_k\|_F^2, \\ &= -\frac{\gamma - L}{2} \|\mathbf{z}_{k+1} - \mathbf{z}_k\|_F^2, \end{aligned}$$

where the last equality follows from the first-order optimality condition for (3.9).

The remainder of the proof of this lemma follows along similar lines to the proof of [13, Lemma 1, p. 470]. ■

The following lemma shows that the augmented Lagrangian has a sufficient decrease in each iteration and it is uniformly lower bounded.

Lemma 3. *Let $\{\mathcal{T}_k\}_{k \geq 0}$ be a sequence generated by [Algorithm 3.1](#) and set*

$$\begin{aligned} \mathcal{D}_k &= \left(\sum_{n=1}^N \|\mathbf{U}_k^{(n)} - \mathbf{U}_{k+1}^{(n)}\|_F^2 \right) + \|\mathcal{G}_k - \mathcal{G}_{k+1}\|_F^2 \\ (.17) \quad &+ \|\mathcal{H}_k - \mathcal{H}_{k+1}\|_F^2 + \|\mathbf{z}_k - \mathbf{z}_{k+1}\|_F^2 + \|\mathbf{y}_k - \mathbf{y}_{k+1}\|_F^2. \end{aligned}$$

Then, there exists a positive constant ϑ such that

$$(.18) \quad \mathcal{L}(\mathcal{T}_{k+1}) \leq \mathcal{L}(\mathcal{T}_k) - \frac{\vartheta}{2} \mathcal{D}_k, \quad \text{for all } k \geq 0,$$

and

$$(.19) \quad \mathcal{D}_k \leq \frac{2}{\vartheta} (\mathcal{L}(\mathcal{T}_0) - \underline{\mathcal{L}}),$$

where $\underline{\mathcal{L}}$ is the uniform lower bound of $\mathcal{L}(\mathcal{T}_k)$.

Proof. Combine (1) with (3.10) to obtain

$$\begin{aligned} \mathbf{y}_{k+1} &= \mathbf{y}_k - \gamma \left((\mathcal{G}_{k+1} + \mathcal{H}_{k+1}) \times_1 \mathbf{U}_{k+1}^{(1)} \cdots \times_N \mathbf{U}_{k+1}^{(N)} - \mathbf{z}_{k+1} \right) \\ (.20) \quad &= \nabla F(s^h, \mathbf{x}; \mathbf{z}_{k+1}). \end{aligned}$$

Now, using [Assumption 2.2](#), we have

$$\begin{aligned} \|\mathbf{y}_{k+1} - \mathbf{y}_k\|_F &\leq \|\nabla F(s^h, \mathbf{x}; \mathbf{z}_{k+1}) - \nabla F(s^h, \mathbf{x}; \mathbf{z}_k)\|_F \\ (.21) \quad &\leq L \|\mathbf{z}_{k+1} - \mathbf{z}_k\|_F. \end{aligned}$$

Hence, we obtain

$$(.22) \quad \mathcal{L}(\mathcal{T}_k^{\mathbf{y}_k}) - \mathcal{L}(\mathcal{T}_{k+1}^{\mathbf{y}_{k+1}}) \geq \frac{1}{\gamma} \|\mathbf{y}_{k+1} - \mathbf{y}_k\|_F^2 \geq -\frac{L^2}{\gamma} \|\mathbf{z}_{k+1} - \mathbf{z}_k\|_F^2.$$

Let $\bar{\gamma} = \frac{\gamma^2 - \gamma L - 2L^2}{2\gamma}$ and

$$(.23) \quad \begin{aligned} \hat{\gamma} &= \max(\varrho^h - L^h, \varrho^g - L^g, \varrho^{(1)} - L^{(1)}, \dots, \varrho^{(n)} - L^{(n)}), \\ \vartheta &= \max(\hat{\gamma}, \bar{\gamma}), \end{aligned}$$

where γ is a dual step-size.

We note that the roots of the quadratic equation $\gamma^2 - \gamma L - 2L^2 = 0$ are $-L$ and $2L$. Hence, our choice of dual step size ($\gamma > 2L$) and regularization parameters in [Algorithm 3.1](#) implies that $\vartheta > 0$. Now, using [Lemma .2](#), and [\(.22\)](#), we have

$$\begin{aligned} \mathcal{L}(\mathcal{T}_k) - \mathcal{L}(\mathcal{T}_{k+1}) &\geq \sum_{n=1}^N \frac{\varrho^n - L^n}{2} \|\mathbf{U}_k^{(n)} - \mathbf{U}_k^{(n+1)}\|_F^2 \\ &\quad + \frac{\varrho^h - L^h}{2} \|\mathcal{H}_k - \mathcal{H}_{k+1}\|_F^2 + \frac{\varrho^g - L^g}{2} \|\mathcal{G}_k - \mathcal{G}_{k+1}\|_F^2 \\ &\quad + \frac{\gamma - L}{2} \|\mathbf{z}_k - \mathbf{z}_{k+1}\|_F^2 - \frac{L^2}{\gamma} \|\mathbf{z}_{k+1} - \mathbf{z}_k\|_F^2 \\ &\geq \frac{\hat{\gamma}}{2} \left(\sum_{n=1}^N \|\mathbf{U}_k^{(n)} - \mathbf{U}_{k+1}^{(n)}\|_F^2 + \|\mathcal{H}_k - \mathcal{H}_{k+1}\|_F^2 + \|\mathcal{G}_k - \mathcal{G}_{k+1}\|_F^2 \right) \\ &\quad + \frac{\gamma^2 - \gamma L - 2L^2}{2\gamma} \cdot \frac{1}{2} (\|\mathbf{z}_k - \mathbf{z}_{k+1}\|_F^2 + \|\mathbf{z}^k - \mathbf{z}_{k+1}\|_F^2) \\ &\geq \frac{\vartheta}{2} \left(\sum_{n=1}^N \|\mathbf{U}_k^{(n)} - \mathbf{U}_k^{(n+1)}\|_F^2 + \|\mathcal{H}_k - \mathcal{H}_{k+1}\|_F^2 + \|\mathcal{G}_k - \mathcal{G}_{k+1}\|_F^2 \right. \\ &\quad \left. + \|\mathbf{z}_k - \mathbf{z}_{k+1}\|_F^2 + \|\mathbf{y}_k - \mathbf{y}_{k+1}\|_F^2 \right). \end{aligned}$$

where the last inequality follows from [\(.23\)](#).

To show [\(.19\)](#), let $\tilde{\mathbf{z}} = (\mathcal{G} + \mathcal{H}) \times_1 \mathbf{U}^{(1)} \cdots \times_N \mathbf{U}^{(N)}$. Using [Assumption 2.2](#), we have

$$\begin{aligned} F(s^h, \mathbf{x}; \tilde{\mathbf{z}}_{k+1}) &\leq F(s^h, \mathbf{x}; \mathbf{z}_k) + \langle \nabla F(s^h, \mathbf{x}; \mathbf{z}_{k+1}), \tilde{\mathbf{z}}_{k+1} - \mathbf{z}_{k+1} \rangle \\ &\quad + \frac{L}{2} \|\tilde{\mathbf{z}}_{k+1} - \mathbf{z}_{k+1}\|_F^2, \\ (.24) \quad &= F(s^h, \mathbf{x}; \mathbf{z}_k) + \langle \mathbf{y}, \tilde{\mathbf{z}}_{k+1} - \mathbf{z}_{k+1} \rangle + \frac{L}{2} \|\tilde{\mathbf{z}}_{k+1} - \mathbf{z}_{k+1}\|_F^2, \end{aligned}$$

By [Assumption 4.1](#), penalty functions $\{J_1(\cdot), J_2(\cdot), J_{3,1}(\cdot), J_{3,2}(\cdot), \dots, J_{3,N}(\cdot)\}$ and the loss function F are lower bounded. Now, since $\gamma > L$, there must exists a constant $\underline{\mathcal{L}}$, such that

$$\begin{aligned} (.25) \quad \mathcal{L}(\mathcal{T}_{k+1}) &\geq F(s^h, \mathbf{x}; \tilde{\mathbf{z}}_{k+1}) + \lambda_1 J_1(\mathcal{G}_{k+1}) + \lambda_2 J_2(\mathcal{G}_{k+1}) \\ &\quad + \lambda_3 J_3(\mathbf{U}_{k+1}) + \frac{\gamma - L}{2} \|\tilde{\mathbf{z}}_{k+1} - \mathbf{z}_{k+1}\|_F^2, \\ &\geq \underline{F} + \underline{J}_1 + \underline{J}_2 + \underline{J}_3 \geq \underline{\mathcal{L}}. \end{aligned}$$

Now, using (.18), we get (.19). ■

Next, we give a formal definition of the limit point set. Let the sequence $\{\mathcal{T}_k\}_{k \geq 0}$ be a sequence generated by the Algorithm 3.1 from a starting point \mathcal{T}_0 . The set of all limit points is denoted by $\Upsilon(\mathcal{T}_0)$, i.e.,

$$\Upsilon(\mathcal{T}_0) = \{\bar{\mathcal{T}} : \exists \text{ an infinite sequence } \{\mathcal{T}_{k_s}\}_{s \geq 0} \text{ such that } \mathcal{T}_{k_s} \rightarrow \bar{\mathcal{T}} \text{ as } s \rightarrow \infty\}.$$

Next, we show that the set of accumulations points of the sequence $\{\mathcal{T}_k\}_{k \geq 0}$ generated by Algorithm 3.1 is nonempty and it is a subset of the critical points of \mathcal{L} .

Lemma 4. *Let $\{\mathcal{T}_k\}_{k \geq 0}$ be a sequence generated by Algorithm 3.1. Then,*

- (i) $\Upsilon(\mathcal{T}_0)$ is a non-empty set, and any point in $\Upsilon(\mathcal{T}_0)$ is a critical point of $\mathcal{L}(\mathcal{T})$;
- (ii) $\Upsilon(\mathcal{T}_0)$ is a compact and connected set;
- (iii) The function $\mathcal{L}(\mathcal{T})$ is finite and constant on $\Upsilon(\mathcal{T}_0)$.

Proof. (i). It follows from (.19) that the sequence $\{\mathcal{T}_k\}_{k \geq 0}$ is bounded which implies that $\Upsilon(\mathcal{T}_0)$ is non-empty due to the Bolzano-Weierstrass Theorem. Consequently, there exists a sub-sequence $\{\mathcal{T}_{k_s}\}_{s \geq 0}$, such that

$$(\text{.26}) \quad \mathcal{T}_{k_s} \rightarrow \mathcal{T}_*, \quad \text{as } s \rightarrow \infty.$$

Since $J_{3,n}$ is lower semi-continuous, (.26) yields

$$(\text{.27}) \quad \liminf_{s \rightarrow \infty} J_{3,n}(\mathbf{U}_{k_s}^{(n)}) \geq J_{3,n}(\mathbf{U}_*^{(n)}).$$

Further, from the iterative step (.3.12), we have

$$\mathbf{U}_{k+1}^{(n)} = \underset{\mathbf{U}^{(n)}}{\operatorname{argmin}} \quad \lambda_{3,n} J_{3,n}(\mathbf{U}^{(n)}) + \langle \nabla_{\mathbf{U}^{(n)}} \bar{\mathcal{L}}(\mathcal{T}_k^{\mathbf{U}_k^{(n)}}), \mathbf{U}^{(n)} - \mathbf{U}_k^{(n)} \rangle + \frac{\varrho^n}{2} \|\mathbf{U}^{(n)} - \mathbf{U}_k^{(n)}\|_F^2,$$

Thus, letting $\mathbf{U}^{(n)} = \mathbf{U}_*^{(n)}$ in the above, we get

$$\begin{aligned} & \lambda_{3,n} J_{3,n}(\mathbf{U}_{k+1}^{(n)}) + \langle \nabla_{\mathbf{U}^{(n)}} \bar{\mathcal{L}}(\mathcal{T}_k^{\mathbf{U}_k^{(n)}}), \mathbf{U}_{k+1}^{(n)} - \mathbf{U}_k^{(n)} \rangle + \frac{\varrho^n}{2} \|\mathbf{U}_{k+1}^{(n)} - \mathbf{U}_k^{(n)}\|_F^2, \\ (\text{.28}) \quad & \leq \lambda_{3,n} J_{3,n}(\mathbf{U}_*^{(n)}) + \langle \nabla_{\mathbf{U}^{(n)}} \bar{\mathcal{L}}(\mathcal{T}_k^{\mathbf{U}_k^{(n)}}), \mathbf{U}_*^{(n)} - \mathbf{U}_k^{(n)} \rangle + \frac{\varrho^n}{2} \|\mathbf{U}_*^{(n)} - \mathbf{U}_k^{(n)}\|_F^2, \end{aligned}$$

Choosing $k = k_s - 1$ in the above inequality and letting s goes to ∞ , we obtain

$$(\text{.29}) \quad \limsup_{s \rightarrow \infty} J_{3,n}(\mathbf{U}_{k_s}^{(n)}) \leq J_{3,n}(\mathbf{U}_*^{(n)}).$$

Here, we have used the fact that $\nabla_{\mathbf{U}^{(n)}} \bar{\mathcal{L}}$ is a gradient Lipchitz continuous function w.r.t. $\mathbf{U}^{(n)}$, the sequence $\mathbf{U}_k^{(n)}$ is bounded and that the distance between two successive iterates tends to zero (see, (.19)).

Combine (.27) and (.29) to obtain

$$(\text{.30}) \quad \lim_{s \rightarrow \infty} J_{3,n}(\mathbf{U}_{k_s}^{(n)}) = J_{3,n}(\mathbf{U}_*^{(n)}) \quad \text{for all } n \in N.$$

Arguing similarly with other variables, we obtain

$$(.31) \quad \lim_{s \rightarrow \infty} J_1(\mathcal{G}_{k_s}) = J_1(\mathcal{G}_*),$$

$$(.32) \quad \lim_{s \rightarrow \infty} J_2(\mathcal{H}_{k_s}) = J_2(\mathcal{H}_*),$$

$$(.33) \quad \lim_{s \rightarrow \infty} F(s^h, \mathcal{X}; \mathcal{Z}_{k_s}) = F(s^h, \mathcal{X}; \mathcal{Z}_*),$$

$$(.34) \quad \lim_{s \rightarrow \infty} \bar{\mathcal{L}}(\mathcal{T}_{k_s}) = \bar{\mathcal{L}}(\mathcal{T}^*),$$

where (.31) and (.32) follow since J_1 and J_2 are lower semi-continuous; (.33) and (.34) are obtained from the continuity of functions F and $\bar{\mathcal{L}}$. Thus, $\lim_{s \rightarrow \infty} \mathcal{L}(\mathcal{T}_{k_s}) = \mathcal{L}(\mathcal{T}_*)$.

Next, we show that \mathcal{T}_* is a critical point of $\mathcal{L}(\cdot)$. By the first-order optimality condition for the augmented Lagrangian function in (.3.4), we have

$$\begin{aligned} \partial J_{3,n}(\mathbf{U}_{k+1}^{(n)}) + \nabla_{\mathbf{U}^{(n)}} \bar{\mathcal{L}}(\mathcal{T}_{k+1}^{\mathbf{U}_{k+1}^{(n)}}) &\in \partial_{\mathbf{U}^{(n)}} \mathcal{L}(\mathbf{U}_{k+1}^{(n)}), \quad n = 1, \dots, N, \\ \partial J_2(\mathcal{H}_{k+1}) + \nabla_{\mathcal{H}} \bar{\mathcal{L}}(\mathcal{T}_{k+1}^{\mathcal{H}_{k+1}}) &\in \partial_{\mathcal{H}} \mathcal{L}(\mathcal{H}_{k+1}), \\ \partial J_1(\mathcal{G}_{k+1}) + \nabla_{\mathcal{G}} \bar{\mathcal{L}}(\mathcal{T}_{k+1}^{\mathcal{G}_{k+1}}) &\in \partial_{\mathcal{G}} \mathcal{L}(\mathcal{G}_{k+1}), \\ \nabla_{\mathcal{Z}} F(s^h, \mathcal{X}; \mathcal{Z}_{k+1}) + \nabla_{\mathcal{Z}} \bar{\mathcal{L}}(\mathcal{T}_{k+1}^{\mathcal{Z}_{k+1}}) &= \nabla_{\mathcal{Z}} \mathcal{L}(\mathcal{Z}_{k+1}), \\ (.35) \quad \gamma((\mathcal{G}_{k+1} + \mathcal{H}_{k+1}) \times_1 \mathbf{U}_{k+1}^{(1)} \cdots \times_N \mathbf{U}_{k+1}^{(N)} - \mathcal{Z}_{k+1}) &= -\nabla_{\mathcal{Y}} \mathcal{L}(\mathcal{Y}^{k+1}). \end{aligned}$$

Similarly, by the first-order optimality condition for subproblems (.3.12), (.3.13), (.3.14) and (.3.9), we have

$$\begin{aligned} \partial J_{3,n}(\mathbf{U}_{k+1}^{(n)}) + \nabla_{\mathbf{U}^{(n)}} \bar{\mathcal{L}}(\mathcal{T}_k^{\mathbf{U}_{k+1}^{(n)}}) + \rho^{(n)}(\mathbf{U}_k^{(n)} - \mathbf{U}_{k+1}^{(n)}) &= 0, \quad n = 1, \dots, N, \\ \partial J_2(\mathcal{H}_{k+1}) + \nabla_{\mathcal{H}} \bar{\mathcal{L}}(\mathcal{T}_k^{\mathcal{H}_{k+1}}) + \rho^{\mathcal{H}}(\mathcal{H}_k - \mathcal{H}_{k+1}) &= 0, \\ \partial J_1(\mathcal{G}_{k+1}) + \nabla_{\mathcal{G}} \bar{\mathcal{L}}(\mathcal{T}_k^{\mathcal{G}_{k+1}}) + \rho^{\mathcal{G}}(\mathcal{G}_k - \mathcal{G}_{k+1}) &= 0, \\ (.36) \quad \nabla_{\mathcal{Z}} F(s^h, \mathcal{X}; \mathcal{Z}_{k+1}) &= 0. \end{aligned}$$

Combine (.35) with (.36) to obtain

$$(.37) \quad (\xi_{k+1}^1, \dots, \xi_{k+1}^N, \xi_{k+1}^{\mathcal{G}}, \xi_{k+1}^{\mathcal{H}}, \xi_{k+1}^{\mathcal{Z}}, \xi_{k+1}^{\mathcal{Y}}) \in \partial \mathcal{L}(\mathcal{T}_{k+1}),$$

where

$$\begin{aligned} \xi_{\mathbf{U}^{(n)}}^{k+1} &:= \nabla_{\mathbf{U}^{(n)}} \bar{\mathcal{L}}(\mathcal{T}_{k+1}^{\mathbf{U}_{k+1}^{(n)}}) - \nabla_{\mathbf{U}^{(n)}} \bar{\mathcal{L}}(\mathcal{T}_k^{\mathbf{U}_{k+1}^{(n)}}) - \rho^{(n)}(\mathbf{U}_k^{(n)} - \mathbf{U}_{k+1}^{(n)}), \quad n = 1, \dots, N, \\ \xi_{\mathcal{H}}^{k+1} &:= \nabla_{\mathcal{H}} \bar{\mathcal{L}}(\mathcal{T}_{k+1}^{\mathcal{H}_{k+1}}) - \nabla_{\mathcal{H}} \bar{\mathcal{L}}(\mathcal{T}_k^{\mathcal{H}_{k+1}}) - \rho^{\mathcal{H}}(\mathcal{H}_k - \mathcal{H}_{k+1}), \\ \xi_{\mathcal{G}}^{k+1} &:= \nabla_{\mathcal{G}} \bar{\mathcal{L}}(\mathcal{T}_{k+1}^{\mathcal{G}_{k+1}}) - \nabla_{\mathcal{G}} \bar{\mathcal{L}}(\mathcal{T}_k^{\mathcal{G}_{k+1}}) - \rho^{\mathcal{G}}(\mathcal{G}_k - \mathcal{G}_{k+1}), \\ \xi_{\mathcal{Z}}^{k+1} &:= \nabla_{\mathcal{Z}} \bar{\mathcal{L}}(\mathcal{T}_{k+1}^{\mathcal{Z}_{k+1}}) = \mathcal{Y}_k - \mathcal{Y}_{k+1}, \\ (.38) \quad \xi_{\mathcal{Y}}^{k+1} &:= \frac{1}{\gamma}(\mathcal{Y}_k - \mathcal{Y}_{k+1}). \end{aligned}$$

Note that the function $\bar{\mathcal{L}}(\mathcal{T})$ defined in (3.11) is a gradient Lipchitz continuous function w.r.t. $\mathbf{U}^{(1)}, \dots, \mathbf{U}^{(N)}, \mathcal{G}, \mathcal{H}$. Thus,

$$\begin{aligned}
 \|\nabla_{\mathbf{U}^{(n)}} \bar{\mathcal{L}}(\mathcal{T}_{k+1}^{\mathbf{U}_{k+1}^{(n)}}) - \nabla_{\mathbf{U}^{(n)}} \bar{\mathcal{L}}(\mathcal{T}_k^{\mathbf{U}_k^{(n)}})\| &\leq \rho^{(n)} \|\mathbf{U}_k^{(n)} - \mathbf{U}_{k+1}^{(n)}\|, \quad n = 1, \dots, N, \\
 \|\nabla_{\mathcal{H}} \bar{\mathcal{L}}(\mathcal{T}_{k+1}^{\mathcal{H}_{k+1}}) - \nabla_{\mathcal{H}} \bar{\mathcal{L}}(\mathcal{T}_k^{\mathcal{H}_k})\| &\leq \rho^{\mathcal{H}} \|\mathcal{H}_k - \mathcal{H}_{k+1}\|, \\
 \|\nabla_{\mathcal{G}} \bar{\mathcal{L}}(\mathcal{T}_{k+1}^{\mathcal{G}_{k+1}}) - \nabla_{\mathcal{G}} \bar{\mathcal{L}}(\mathcal{T}_k^{\mathcal{G}_k})\| &\leq \rho^{\mathcal{G}} \|\mathcal{G}_k - \mathcal{G}_{k+1}\|,
 \end{aligned}
 \tag{.39}$$

Using (.39), (.19) and (.38), we obtain

$$\lim_{k \rightarrow \infty} (\|\xi_{k+1}^1\|, \dots, \|\xi_{k+1}^N\|, \|\xi_{k+1}^{\mathcal{G}}\|, \|\xi_{k+1}^{\mathcal{H}}\|, \|\xi_{k+1}^{\mathcal{Z}}\|, \|\xi_{k+1}^{\mathcal{Y}}\|) = (0, \dots, 0).
 \tag{.40}$$

Now, from (.37) and (.40), we conclude that $(0, \dots, 0) \in \partial \mathcal{L}(\mathcal{T}_*)$ due to the closedness property of $\partial \mathcal{L}$. Therefore, \mathcal{T}_* is a critical point of $\mathcal{L}(\cdot)$. This completes the proof of (i).

(ii). The proof follows from [13, Lemma 5 and Remark 5].

(iii). Let $\mathcal{L}_* = \lim_{k \rightarrow \infty} \mathcal{L}(\mathcal{T}_k)$. Choose $\mathcal{T}_* \in \Upsilon(\mathcal{T}_0)$. There exists a subsequence \mathcal{T}_{k_s} converging to \mathcal{T}_* as s goes to infinity. Since we have proven that $\lim_{s \rightarrow \infty} \mathcal{L}(\mathcal{T}_{k_s}) = \mathcal{L}(\mathcal{T}_*)$, and $\mathcal{L}(\mathcal{T}_k)$ is a non-increasing sequence, we conclude that $\mathcal{L}(\mathcal{T}_*) = \mathcal{L}_*$, hence the restriction of $\mathcal{L}(\mathcal{T})$ to $\Upsilon(\mathcal{T}_0)$ equals \mathcal{L}_* . \blacksquare

.0.5. Proof of Theorem 3.2. The augmented Lagrangian function $\mathcal{L}(\mathcal{T})$ is a Kurdyka-Lojasiewicz function. Further, by Lemma .4, $\mathcal{L}(\mathcal{T})$ is constant on $\Upsilon(\mathcal{T}_0)$ and $\Upsilon(\mathcal{T}_0)$ is compact. Putting all these together, the proof of this theorem follows along similar lines to the proof of [14, Theorem 1], with function $\psi(x)$ replaced by $\mathcal{L}(\mathcal{T})$.

Appendix D: Consistency of DCOT (Proof of Theorem 4.3). We bound empirical processes induced by $\rho(\cdot, \cdot)$ defined in (4.1) by a chaining argument as [88, 68]. We define a partition of $\Gamma(\mathcal{Z})$ (the parameter space of \mathcal{Z}) as follows

$$A(\zeta) = \{\mathcal{Z} \in \Gamma(\mathcal{Z}) : \zeta \leq \rho(\mathcal{Z}^*, \mathcal{Z}) \leq 2\zeta\}.
 \tag{.41}$$

Since $\hat{\mathcal{Z}}$ is the minimizer of (2.3),

$$\begin{aligned}
 &P\left(\rho(\hat{\mathcal{Z}}, \mathcal{Z}^*) \geq \eta\right) \\
 &\leq P^*\left(\sup_{\mathcal{Z} \in \bigcup_{\zeta} A(\zeta)} (F(s^h, \mathcal{X}; \mathcal{Z}^*) - F(s^h, \mathcal{X}; \mathcal{Z}) + \lambda(J(\mathcal{Z}^*) - J(\mathcal{Z}))) \geq 0\right).
 \end{aligned}
 \tag{.42}$$

where P^* denote the outer probability measure [11]. We obtain an upper bound for the loss difference f_Δ as follows

$$\begin{aligned}
f_\Delta &= f(s_{i_1 \dots i_N}^h, z_{i_1 \dots i_N}, x_{i_1 \dots i_N}) - f(s_{i_1 \dots i_N}^h, z_{i_1 \dots i_N}^*, x_{i_1 \dots i_N}) \\
&= \sum_{j_1, \dots, j_N \in \Omega} s_{i_1 \dots i_N, j_1 \dots j_N}^h (z_{i_1 \dots i_N} - z_{i_1 \dots i_N}^*) \cdot (2x_{j_1 \dots j_N} - z_{i_1 \dots i_N}^* - z_{i_1 \dots i_N}) \\
&= \sum_{j_1, \dots, j_N \in \Omega} 2s_{i_1 \dots i_N, j_1 \dots j_N}^h (z_{i_1 \dots i_N} - z_{i_1 \dots i_N}^*) (z_{j_1 \dots j_N}^* - z_{i_1 \dots i_N}^*) \\
&+ \sum_{j_1, \dots, j_N} 2s_{i_1 \dots i_N, j_1 \dots j_N}^h (z_{i_1 \dots i_N} - z_{i_1 \dots i_N}^*) \varepsilon_{j_1 \dots j_N} - (z_{i_1 \dots i_N}^* - z_{i_1 \dots i_N})^2, \\
&\leq a_1 \sqrt{R_{\min}} |z_{i_1 \dots i_N}^* - z_{i_1 \dots i_N}| \underbrace{\sum_{j_1, \dots, j_N \in \Omega} 2s_{i_1 \dots i_N, j_1 \dots j_N}^h d(y_{i_1 \dots i_N}, y_{j_1 \dots j_N})^\alpha}_{T_1}, \\
(.43) \quad &+ \underbrace{\sum_{j_1, \dots, j_N \in \Omega} 2s_{i_1 \dots i_N, j_1 \dots j_N}^h (z_{i_1 \dots i_N} - z_{i_1 \dots i_N}^*) \varepsilon_{j_1 \dots j_N}}_{T_2} - \underbrace{(z_{i_1 \dots i_N}^* - z_{i_1 \dots i_N})^2}_{T_3}.
\end{aligned}$$

where the second inequality follows from [Assumption 4.1](#).

Individual terms in (.43) can be bounded in the following way: From (.41), for any $\mathbf{z} \in A(\zeta)$, we have

$$(.44) \quad \zeta^2 \leq \frac{1}{\prod_{n \in [N]} I_n} \sum_{i_1=1}^{I_1} \dots \sum_{i_N=1}^{I_N} T_3 \leq 4\zeta^2.$$

This together with the Cauchy-Schwarz inequality implies

$$\begin{aligned}
\frac{1}{\prod_{n \in [N]} I_n} \sum_{i_1=1}^{I_1} \dots \sum_{i_N=1}^{I_N} T_1 &\leq \left(\frac{1}{\prod_{n \in [N]} I_n} \sum_{i_1=1}^{I_1} \dots \sum_{i_N=1}^{I_N} (z_{i_1 \dots i_N} - z_{i_1 \dots i_N}^*)^2 \right)^{1/2} \\
&\left(\frac{1}{\prod_{n \in [N]} I_n} \sum_{i_1=1}^{I_1} \dots \sum_{i_N=1}^{I_N} \left(\sum_{j_1, \dots, j_N \in \Omega} 2s_{i_1 \dots i_N, j_1 \dots j_N}^h d(y_{i_1 \dots i_N}, y_{j_1 \dots j_N})^\alpha \right)^2 \right)^{1/2}.
\end{aligned}$$

Now, using (.41) and [Assumption 4.1](#), we have

$$(.45) \quad \sup_{A(\zeta)} \frac{1}{\prod_{n \in [N]} I_n} \sum_{i_1=1}^{I_1} \dots \sum_{i_N=1}^{I_N} T_1 \leq 4\zeta a_1 \sqrt{R_{\min}} h^{-\alpha}.$$

In order to bound T_2 , from (.43) and (.44), we obtain

$$\begin{aligned} \frac{1}{\prod_{n \in [N]} I_n} \sum_{i_1=1}^{I_1} \cdots \sum_{i_N=1}^{I_N} T_2 &\leq \frac{1}{\prod_{n \in [N]} I_n} \sum_{i_1=1}^{I_1} \cdots \sum_{i_N=1}^{I_N} \left(\sum_{j_1, \dots, j_N \in \Omega} 2s_{i_1 \dots i_N, j_1 \dots j_N}^h (z_{i_1 \dots i_N} - z_{i_1 \dots i_N}^*) \varepsilon_{j_1 \dots j_N} \right) \\ &\leq \left(\frac{1}{\prod_{n \in [N]} I_n} \sum_{i_1=1}^{I_1} \cdots \sum_{i_N=1}^{I_N} (z_{i_1 \dots i_N} - z_{i_1 \dots i_N}^*)^2 \right)^{1/2} \\ &\quad \left(\frac{1}{\prod_{n \in [N]} I_n} \sum_{i_1=1}^{I_1} \cdots \sum_{i_N=1}^{I_N} \left(\sum_{j_1, \dots, j_N \in \Omega} 2s_{i_1 \dots i_N, j_1 \dots j_N}^h \varepsilon_{j_1 \dots j_N} \right)^2 \right)^{1/2}. \end{aligned}$$

where the second inequality is obtained from Cauchy-Schwarz inequality. Combine the above inequality with (.44) to obtain

$$\begin{aligned} &\sup_{A(\zeta)} \frac{1}{\prod_{n \in [N]} I_n} \sum_{i_1=1}^{I_1} \cdots \sum_{i_N=1}^{I_N} T_2 \\ (.46) \quad &\leq \zeta \left(\frac{1}{\prod_{n \in [N]} I_n} \sum_{i_1=1}^{I_1} \cdots \sum_{i_N=1}^{I_N} \left(\sum_{j_1, \dots, j_N \in \Omega} 2s_{i_1 \dots i_N, j_1 \dots j_N}^h \varepsilon_{j_1 \dots j_N} \right)^2 \right)^{1/2}. \end{aligned}$$

Let

$$(.47) \quad Q_\zeta := \frac{\zeta^2 - 4\zeta a_1 \sqrt{R_{\min}} h^{-\alpha} - \lambda J(\mathbf{Z}^*)}{\zeta}.$$

Then, from (.44), (.45) and (.46), for each ζ , we have

$$\begin{aligned} &P^* \left(\sup_{A(\zeta)} (F(s^h, \mathbf{X}; \mathbf{Z}^*) - F(s^h, \mathbf{X}; \mathbf{Z})) \geq \lambda (J(\mathbf{Z}) - J(\mathbf{Z}^*)) \right) \\ &\leq P^* \left(\left(\frac{1}{\prod_{n \in [N]} I_n} \sum_{i_1=1}^{I_1} \cdots \sum_{i_N=1}^{I_N} \left(\sum_{j_1, \dots, j_N \in \Omega} 2s_{i_1 \dots i_N, j_1 \dots j_N}^h \varepsilon_{j_1 \dots j_N} \right)^2 \right)^{1/2} \geq Q_\zeta \right) \\ &\leq P^* \left(\max_{i_1, \dots, i_N} \left| \sum_{j_1, \dots, j_N \in \Omega} 2s_{i_1 \dots i_N, j_1 \dots j_N}^h \varepsilon_{j_1 \dots j_N} \right| \geq Q_\zeta \right) \\ &\leq \sum_{i_1=1}^{I_1} \cdots \sum_{i_N=1}^{I_N} 2 \exp \left(- \frac{Q_\zeta^2}{2\sigma^2 \max_{i_1, \dots, i_N} \sum_{j_1, \dots, j_N \in \Omega} (s_{i_1 \dots i_N, j_1 \dots j_N}^h)^2} \right) \\ (.48) \quad &\leq 2 \prod_{n \in [N]} I_n \exp \left(- \frac{Q_\zeta^2 h^\beta |\Omega|}{2\sigma^2} \right), \end{aligned}$$

where the third to the last inequalities follow from the Chernoff inequality of a weighted sub-Gaussian distribution [20].

Let $\zeta = 2^{t-1}\eta$. Then (.47) together with our assumptions $\eta \geq 2^4 a_1 \sqrt{R_{\min}} h^\alpha$, $\lambda J(\mathbf{Z}^*) \leq 2^{-2}\eta^2$ and (.48) implies

$$\begin{aligned} & \sum_{t=1}^{\infty} P^* \left(\sup_{A(2^{t-1}\eta)} (F(s^h, \mathbf{X}; \mathbf{Z}^*) - F(s^h, \mathbf{X}; \mathbf{Z})) \geq \lambda J(\mathbf{Z}) - \lambda J(\mathbf{Z}^*) \right) \\ & \leq 4 \prod_{n \in [N]} I_n \sum_{t=1}^{\infty} \exp\left(-\frac{h^\beta |\Omega| 2^{2t-8} \eta^2}{2\sigma^2}\right) \\ & \leq 4 \prod_{n \in [N]} I_n \frac{\exp(-a_2 \frac{h^\beta |\Omega| \eta^2}{\sigma^2})}{1 - \exp(-a_2 \frac{h^\beta |\Omega| \eta^2}{\sigma^2})}, \end{aligned}$$

where $a_2 > 0$ is a constant.

Thus, there exists a positive constant a_3 such that

$$P(\rho(\hat{\mathbf{Z}}, \mathbf{Z}^*) \geq \eta) \leq a_3 \exp(-a_2 \frac{h^\beta |\Omega| \eta^2}{\sigma^2}) + \log \prod_{n \in [N]} I_n.$$